SURFACE STUDIES RELATED TO THE DEVELOPMENT OF A HYPERTHERMAL OXYGEN ATOM BEAM GENERATOR

By

MARK ROGERS DAVIDSON

A DISSERTATION PRESENTED TO THE GRADUATE SCHOOL
OF THE UNIVERSITY OF FLORIDA IN PARTIAL FULFILLMENT
OF THE REQUIREMENTS FOR THE DEGREE OF
DOCTOR OF PHILOSOPHY

UNIVERSITY OF FLORIDA

1990

ACKNOWLEDGMENTS

The author wishes to thank his father and mother, who instilled in him the desire to know how things work, and the confidence to tackle the sometimes difficult and frustrating task of learning how and why the things around us behave the way they do. The author has been ready to give up on a problem many times when he remembered that "F = ma, you can't push on a rope, and the rest is just algebra," as his father told him as he grew up. The author also wishes to thank his wife Jan, who has put up with 6 years of being a graduate student's wife and all of the many inconveniences which that entails. Without her support, these years of education would not have been possible. The author's appreciation goes to both his freshman chemistry professor, Dr. Sam Colgate, and Dr. H.A. Laitinen, in whose laboratory he worked as an undergraduate. These two men, in particular, first showed him how exciting research can be. The author wishes to thank his advisor, Professor Gar B. Hoflund, for having a seemingly infinite amount of patience and helpful guidance during the learning process. Lastly, the author wishes to thank Dr. R.A. Outlaw, who provided the motivation for this work and a great deal of guidance in both the experimental aspects of this work

and in the interpretation of the data. He also thanks Dr. Outlaw for performing the diffusivity and permeability experiments on his permeability apparatus.

TABLE OF CONTENTS

	page
ACKNOWLEDGMENTS	ii
ABSTRACT	iv
INTRODUCTION	1
Motivation	1
Past Research	5
OXYGEN TRANSPORT THROUGH HIGH-PURITY, LARGE-GRAIN SILVER	14
Introduction	14
Permeation Analysis	15
Experimental	18
Results and Discussion	24
Summary	34
A NONDESTRUCTIVE DEPTH PROFILE STUDY OF OXYGEN-EXPOSED, LARGE-GRAIN SILVER USING ARAES AND ISS	36
Introduction	36
Experimental	37
Results and Discussion	42
Conclusions	54
ESD AND SURFACE ANALYSIS STUDIES OF SILVER/0.5% ZIRCONIUM ALLOY	55
Introduction	55
Experimental	58
Results and Discussion	67
Summary and Conclusions	79
APPENDIX DESCRIPTION OF THE ULTRAHIGH VACUUM SURFACE FACILITY	80
REFERENCES	85
BIOGRAPHICAL SKETCH	90

Abstract of Dissertation Presented to the Graduate School of the University of Florida in Partial Fulfillment of the Requirements for the Degree of Doctor of Philosophy

SURFACE STUDIES RELATED TO THE DEVELOPMENT OF A HYPERTHERMAL OXYGEN ATOM BEAM GENERATOR

By

MARK ROGERS DAVIDSON

May, 1990

Chairman: Gar B. Hoflund
Major Department: Chemical Engineering

Silver and silver alloys are important catalytic materials for several commercially important reactions such as ethylene epoxidation. In addition, silver and its alloys have been used as oxygen permeation membranes in the development of an hyperthermal neutral oxygen atom gun. The permeability and diffusivity of oxygen in large-grain, high-purity silver was measured. Both the diffusivity and the permeability were found to be significantly lower than previous investigators have reported. It is believed that grain boundary transport played an important role in previous studies. The silver used in this study had a very low grain boundary density, so the transport rates were slower. This hypothesis is supported by Auger electron spectroscopy (AES) line scans of heated, oxygen-saturated silver which show the oxygen accumulating near the grain boundaries. The apparent

activation energy for diffusion changed near 630 C, possibly indicating some oxygen trapping is occurring. The surface analysis techniques of angle resolved Auger electron spectroscopy (ARAES), X-ray photoelectron spectroscopy (XPS), ion scattering spectroscopy (ISS), and electron stimulated desorption (ESD) have been used to study the chemical interaction and mechanisms of diffusion of oxygen in pure silver and 0.5% zirconium silver alloys. It has been shown that a surface relaxation in the first several silver layers occurs which strongly affects the oxygen concentration profile. Oxygen and zirconium diffusion constants and neutral and positive ion ESD cross sections from the Ag/Zr alloy have also been obtained. A variation of ESD cross section with electron beam incidence angle has been observed and, relative changes with cross section have been measured for several incidence angles.

INTRODUCTION

Motivation

This work was motivated by two seemingly unrelated important industrial problems. The first involves the degradation of materials in orbiting spacecraft due to collision with neutral oxygen atoms. The main objective of this research is to help in the development of a research tool which could be used to study the degradation of proposed spacecraft materials in ground-based laboratories. The second application of the studies presented in this work has to do with the optimization of the catalytic oxidation of ethylene to form ethylene epoxide.

The atmosphere at typical orbital altitudes (200 to 1000 km) consists largely of neutral atomic oxygen atoms. This combined with the large velocity of the orbiting vehicle (≈8 $km\text{-}s^{-1}$) results in a flux of hyperthermal neutral oxygen atoms (E≈5 eV, Flux ≈ 1 x 10^{15} $atoms\text{-}cm^{-2}\text{-}s^{-1}$) colliding with the leading spacecraft surfaces. This highly energetic collision of the atomic oxygen has been a major cause of materials degradation during space shuttle missions [1]. A good example of the problems which this can create was recently seen during the retrieval of the long duration exposure facility satellite

(LDEFS). The planned duration of the satellite was 1 year, after which it would be retrieved and the results of the on-board experiments analyzed. Due to the space shuttle Challenger accident, the retrieval was delayed 3 years. One of the experimental panels on board consisted of a panel of layered polymer films. When the satellite was grasped by the retrieval arm, the panel turned to dust and the results of the experiment were lost. It is believed that the disastrous degradation of the polymer panel was caused by long-term exposure to the hyperthermal oxygen atom flux. Possible problems can also be expected with composite materials proposed for use in the planned space station, exterior coatings of the Hubble Space Telescope, and materials for use in proposed orbiting laser communication systems. Therefore, study of the proposed materials activity towards hyperthermal oxygen in ground-based laboratories is required.

In order to perform these experiments, a source of neutral oxygen atoms with an energy and flux approximating that found in orbit is required. Current schemes for producing neutral oxygen atom fluxes include radio frequency (rf) discharge, thermal dissociation, and electron impact [2]. In order to accelerate these beams to appropriate energies, techniques such as nozzle expansion or charge neutralization are used. These methods generally have several problems which include low flux density, low mean energy, wide energy distribution, and production of excited state atoms. In

addition, these techniques are not generally compatible with the pressure required for a detailed surface analysis. At a typical background pressure for these methods of $\approx 1 \times 10^{-6}$ Torr, the surface which is being studied is covered with background gases in approximately 1 second (assuming a sticking coefficient of nearly 1). Therefore, studies of oxygen-atom-treated surfaces in such systems have been dosed with as much of the background gas (typically CO, CO_2, O_2, and N_2) as the dosing gas. Clearly, any device which is used to produce hyperthermal oxygen atoms must be compatible with vacuum levels in the 10^{-11} Torr range.

Efforts toward producing such a hyperthermal oxygen atom gun (HOAG) have relied on two phenomena. The first is the unusually high permeability of oxygen through silver [1,3,4]. The second is the fact that electron stimulated desorption (ESD) of adsorbates from metal surfaces yields predominantly neutrals with energies in the 3 to 10 eV range [5-26]. The proposed scheme for a continuous HOAG is to pressurize one side of a hot silver membrane with oxygen while the other side of the membrane is exposed to the UHV chamber. The temperature of the membrane is kept below that at which the oxygen will desorb on the vacuum side of the membrane. It has been shown that oxygen diffuses atomically through the silver [27,28]. The silver surface on the vacuum side is then bombarded with electrons, which results in ESD of neutral atomic oxygen with an energy of ≈ 5 eV. A schematic diagram

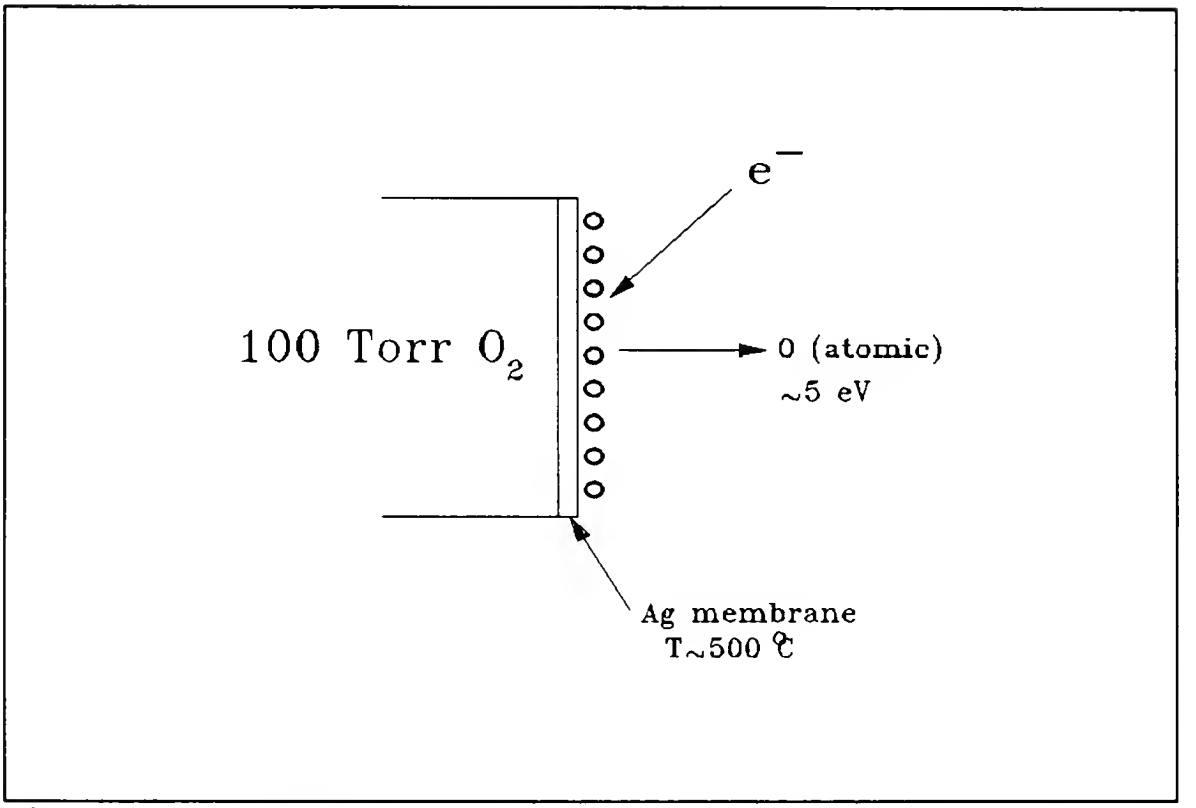

Figure 1. A schematic of the proposed HOAG

of the HOAG is shown in figure 1. Preliminary transient experiments have shown the scheme to be feasible [1].

The second major motivation for studying oxygen interaction with silver and silver alloys is the use of silver as an ethylene epoxidation catalyst. Ethylene epoxide is a commodity chemical which is the precursor to many commercially important chemicals including ethylene glycol (antifreeze). The mechanisms of catalytic ethylene epoxidation by silver have been extensively studied but are still poorly understood [29-69]. Because the volume of ethylene epoxide produced is very large, a small improvement in the catalytic activity or decay rates of the catalyst results in relatively large economic benefits. A great deal of traditional trial and error catalyst optimization has been performed on these catalysts and a fundamental understanding of the mechanisms involved in the reaction and decay in activity of the catalyst are now necessary to further improve the efficiency of the catalyst. An understanding of the adsorption of oxygen on the silver surface and its dissolution into the bulk is a first step in this goal of an improved catalyst design based on an understanding of the fundamentals of the process.

Past Research

As previously mentioned, the basic concept of the HOAG has been tested in a transient experiment [1]. In this experiment, a silver wire was saturated with 10 Torr of oxygen at 500 C for 1 hr. The system was then pumped down to $\approx 10^{-11}$

Torr. The atomic oxygen flux was monitored by a quadrupole mass spectrometer (QMS) which was operated in the appearance potential mode in order to remove any contribution to the 16 AMU signal from fractionation products of CO, CO_2, or other oxygen-containing background gas species. The cross section for ESD was found to be 7×10^{-19} cm^2 and the flux for a surface coverage of 0.5 was found to be 1.1×10^{12} cm^{-2}-s^{-1}. In addition, a diffusivity of 2.64×10^{-6} cm^2-s^{-1} was measured at a temperature of 500°C.

Silver Oxygen Interaction

The majority of the previous research has been conducted on single crystals [37-63] and most of the studies have been performed on the (110) surface since the sticking coefficient ($\approx 10^{-3}$) on that crystal face is about 1000 times greater than on either the (100) or (111) faces [42]. It was found in these studies that molecular oxygen exists on the surface at temperatures below -103°C but that it dissociates and forms adsorbed atomic oxygen above that temperature. Subsurface atomic oxygen is believed to form above 150°C and is stable to about 327°C. Based on low energy electron diffraction measurements, the maximum coverage is believed to be half a monolayer. In addition, a subsurface state has been proposed for the (110) surface, which also desorbs above 327°C.

Polycrystalline studies of the oxygen/silver system are much less common due to the complexity of the results [23,27, 28,64-69]. Polycrystalline samples may show characteristics

of all of the single crystal faces. In addition, defects and grain boundaries can play an important role in the adsorption and diffusion of gasses through solids. The polycrystalline silver studies so far have shown four general oxygen species present after varying exposures. Evidence for a molecular oxygen species has been observed, but this species is not stable at room temperature under vacuum and desorbs quickly. Like the single crystal studies, atomic oxygen was found adsorbed on the surface and dissolved in the bulk. In addition, a strongly-bound oxygen species is formed and it is postulated that this species is associated with grain boundaries and surface imperfections [64].

It is interesting to note that in all of the studies, no molecular oxygen was observed at temperatures above room temperature. X-ray photoelectron spectroscopy (XPS) shows that even though the oxygen is present as atomic oxygen, no silver oxide is formed [27,28]. This indicates that the oxygen forms a solid solution in the silver.

Two reported studies of the surface structure of silver have been found. Ning and coworkers [70] have performed calculations based on the embedded atom method to calculate surface relaxations in a number of materials and crystal planes including the (100),(110), and (111) planes of silver. They show that the (110) and (111) planes undergo an oscillatory relaxation in which the first two atomic layers are contracted, the second two layers are expanded and the

third two layers are contracted. They also provide some experimental results which confirm their findings. Kuk and Feldman [71] have performed high-energy ion scattering/ channelling studies of a silver (110) surface which can give a relatively direct measure of the surface relaxations. They find, in agreement with Moghadam and Stevenson [69] that the surface undergoes an oscillatory relaxation in which the first two layers are contracted and the second two are expanded relative to the bulk layer spacing.

Electron Stimulated Desorption

Electron stimulated desorption has been reviewed by Madey and Yates[5] and more recently by Hoflund[6]. In addition, a large body of research exists which involves studies of systems of various adsorbates on several metal and insulator surfaces [1-23]. Several mechanisms have been proposed for ESD, two of which are predominantly accepted. The first is known as the Menzel-Gomer-Redhead (MGR) model. The MGR process is depicted in Figure 2. The adsorbate vibrates at the ground vibrational state near the bottom of the potential well. The ejection of an electron from a bonding orbital results in the formation of an antibonding orbital which may include either a neutral or ionized particle being ejected. The second mechanism is known as the Knotek-Feibelman (KF) mechanism and differs from the MGR mechanism in the way in which the repulsive potential is created. This mechanism is depicted in Figure 3 for

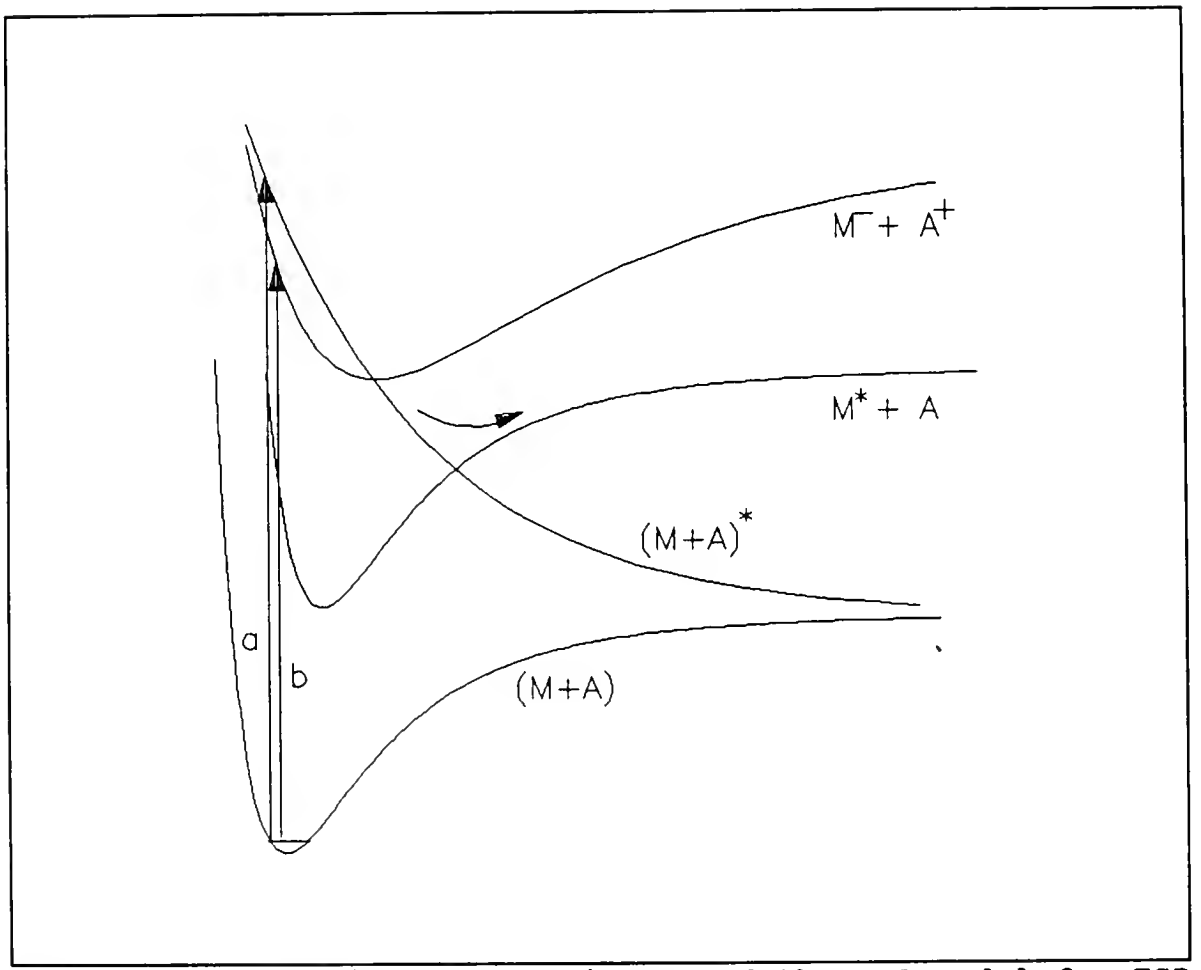

Figure 2. Potential energy diagram of the MGR model for ESD of O ions from TiO_2

desorption of O+ from TiO_2. A core hole in the metal atom created which leaves the molecule in an excited state. One mechanism for de-excitation is an interatomic Auger transition, which removes two or three valence electrons from the oxygen atom. This creates a positively charged oxygen atom next to a positively charged metal atom. The oxygen ion is then ejected by the coulombic force exerted on it. In both the MGR and KF mechanisms, ions desorb and most are neutralized as they leave the surface. Both theoretical and experimental evidence exists which shows that in most cases the ratio of neutrals to ions ranges from 100 to 1000.

Some recent studies of physisorbed adsorbates have shown that nearly all of the desorbed particles are neutral. In these studies, no ions could be detected [20-22,24-26]. Another mechanism has been proposed by Antoniewicz [26] to account for these findings. In this mechanism, a valence electron is ejected from the adsorbate. The potential well for the ion in this case is deeper than that for the neutral adsorbate due possibly to the attraction of the image charge formed in the bulk metal. This attraction causes the ion to move initially towards the surface. As the ion moves closer to the surface, the probability for neutralization increases. When the ion is neutralized, it is no longer in its equilibrium position, and, depending on the position of the ion when it is

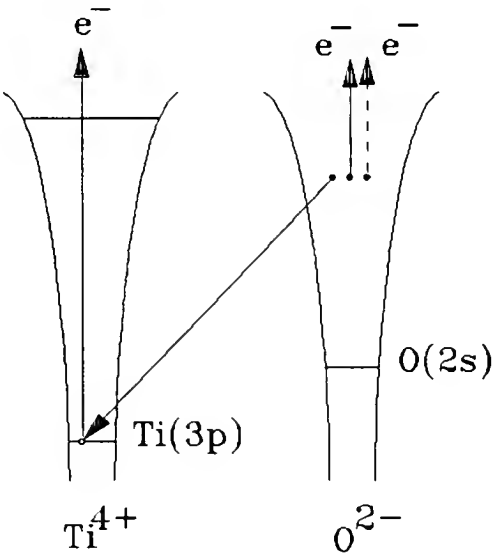

Figure 3. Schematic potential energy diagram of the KF model of the ESD mechanism

neutralized, the atom formed may be high enough on the repulsive portion of the potential energy curve that it can escape the surface and desorb as a neutral atom. In this manner, nearly all of the atoms desorbed are neutral, since desorption depends on neutralization. This mechanism is depicted schematically in Figure 4.

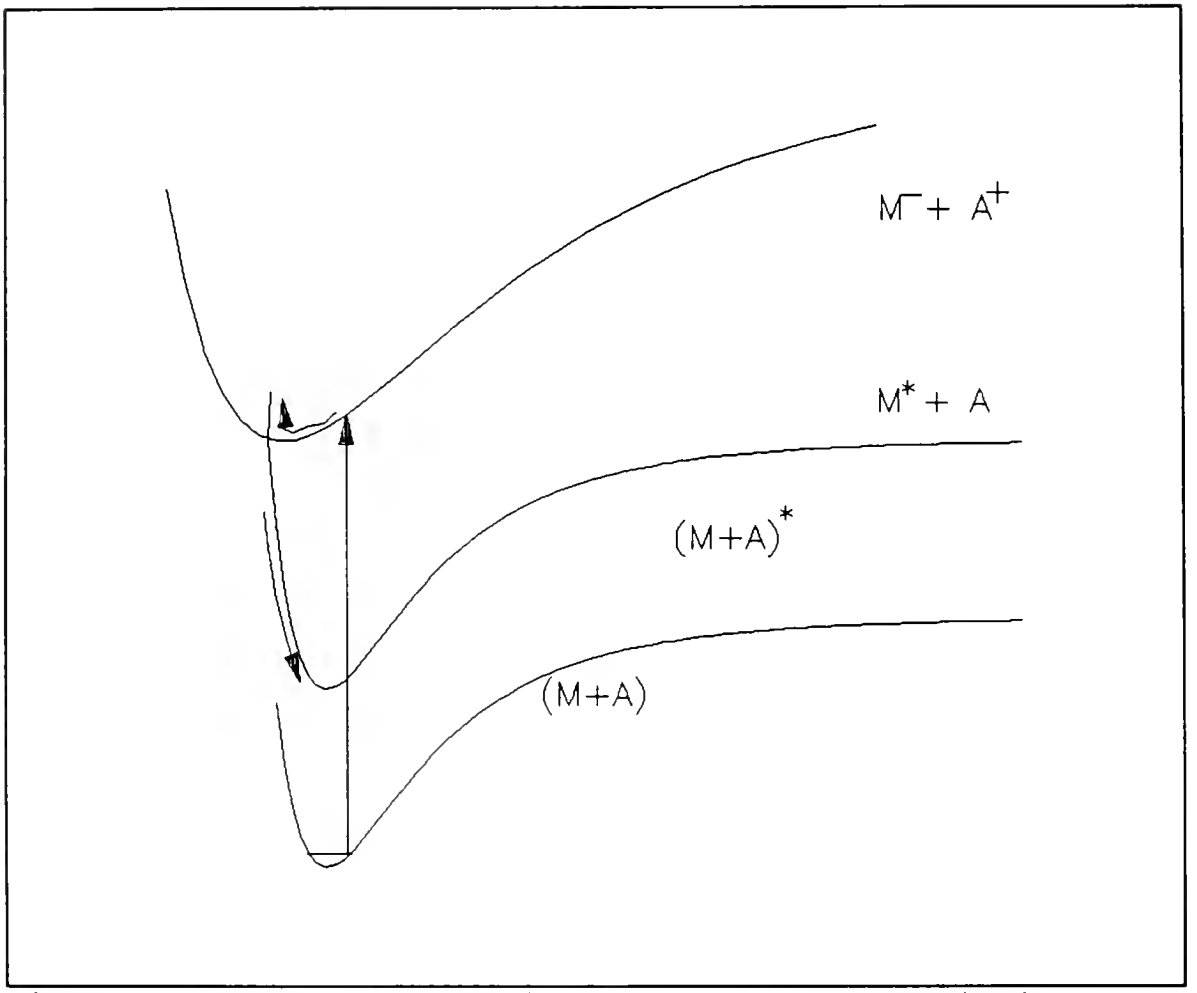

Figure 4. Schematic potential diagram of the Atoniewicz model for the mechanism for ESD of loosely bound adsorbates.

OXYGEN TRANSPORT THROUGH HIGH-PURITY, LARGE-GRAIN SILVER

Introduction

Past measurements of the diffusivity of oxygen in Ag have, in all cases, ignored the effects of grain boundary density and material purity [3,4,72-75]. Since both are important concerns in determining the actual transport mechanism, it is essential that the effects of each be studied. If grain boundary diffusion is a significant part of the transport mechanism for the diffusion of oxygen in Ag, the grain boundary density would have a major effect. Experiments with larger grain size would reduce the number of transport paths and would provide smaller permeation rates compared with past research (which most likely had small grains and therefore higher grain boundary densities). Furthermore, impurities (both species and amounts) could cause oxygen trapping effects that would result in diffusivity variations. Experiments with high-purity Ag would minimize such effects.

This chapter presents results of permeation measurements of oxygen through high-purity, large-grain Ag membranes

conducted under ultrahigh vacuum (UHV) conditions. Auger electron spectroscopy (AES) results of oxygen charged Ag are also presented.

Permeation Analysis

The permeation of planar membranes is generally described in Crank[76]. If a diffusion coefficient D independent of concentration C is assumed, then

$$\frac{\partial C}{\partial t}(x,t) = D \left(\frac{\partial^2 C(x,t)}{\partial x^2}\right) , \qquad (1)$$

where x is the variable distance through the membrane and t is the time.

The boundary conditions applied to this equation can be determined from the permeation process, which includes (a) adsorption of the oxygen molecules on the high-pressure side; (b) dissociation of the molecules to atoms; (c)incorporation of the atoms into the lattice, grain boundaries, or defects; (d) random walk migration through the membrane by means of (c); (e) emergence from a solid solution at the vacuum interface and entry into an adsorbed state; (f) reassociation to molecules; and (g) desorption. Normally the rate controlling step is that of (d).

Following Crank [76], Eq. (1) may be solved using the following boundary conditions:

$$C(x,t=0) = g(x) \qquad (2)$$

$$C(x=0,t) = SP_o^{1/2} = C_1 \ , \qquad (3)$$

$$C(x=d,t) = SP_d^{1/2} = C_2 \ , \qquad (4)$$

where C is concentration, g(x) is and arbitrary function, d is the membrane thickness, S is the solubility, P_o is the high-side pressure, and P_d is the pressure at the UHV interface, which is usually taken to be zero at the beginning of the experiment. Equations (3) and (4) describe the concentration of the gaseous species in the metal assuming that Sievert's law is obeyed. If the upstream side of the membrane is pressurized, then the boundary conditions become $C_1 = SP_o^{1/2}$, $C_2 = 0$ and the gas flux J at steady state is

$$J(x=d,t\to\infty) = DSP_o^{1/2}/d = KP_o^{1/2}/d = J_{ss}, \qquad (5)$$

where the permeability K = DS

The steady-state flux J_{ss} through the membrane is related to the steady-state pressure P_{ss} in the measurement chamber by

$$J_{ss} = P_{ss}f/AkT \ , \qquad (6)$$

where f is the limiting conductance to the main ion pump, k is Boltzmann's constant, T is the gas temperature, and A is the membrane area. The permeability then is

$$K = P_{ss}fd/P_o^{1/2}AkT. \qquad (7)$$

In order to determine the diffusivity following the establishment of a steady-state permeation rate, the upstream of high-pressure side can be reduced to zero such that $C_1=C_2=0$, and the flux becomes

$$J(x=d,t) = \frac{KP_o^{1/2}}{d} \left[-2\sum_{1}^{\infty} (-1)^n \exp\left(-Dn^2\pi^2 t/d^2\right)\right] \quad (8)$$

The time varying flux AJ(t) and pressure P(t) within the measurement system are related by

$$V\frac{dP(t)}{dt} = AkTJ(t) - f[P(t)-P_p(t)] \ , \quad (9)$$

where V is the volume of the measurement chamber and $P_p(t)$ is the time varying pressure within the main pump. The conductance f is chosen such that $P(t) \gg P_p(t)$, and the flux becomes

$$J(t) = \frac{V}{AkT}\frac{dP(t)}{dt} + \frac{f}{AkT}P(t) \quad (10)$$

A comparison of the two terms in Eq. (10) indicates that a worse case condition occurs at high temperatures when dp(t)/dt is greatest, but even at the highest temperature encountered the ratio of the first term to the second term is less than ≈0.02. Therefore, the flux can be simplified to

$$J(t) \approx (f/AkT)P(t). \quad (11)$$

The ratio of Eq. (8) to Eq. (5) combined with Eq. (11) gives

$$\frac{P(t)}{P_{ss}} = -2\sum_{1}^{\infty} (-1)^n \exp\left(-Dn^2\pi^2 t/d^2\right) \ , \quad (12)$$

where D is the diffusivity. Experimentally, the time for $P(t)/P_{ss}$ to decay to some predetermined value can be measured, and then D can be found by numerical iteration of (12).

However, because of the rapid decay of the exponential function, no significant error is introduced by considering only the first terms of the summation.

Experimental

Membrane Preparation

The permeation membranes used in this work (99.999 + % vacuum-melted Ag) were spark machined into a disk geometry that fits between two mini-flanges to separate the UHV detection volume from the oxygen supply volume. The membrane surfaces were prepared by polishing to a 30μm grit finish, followed by degreasing with laboratory detergent in an ultrasonic cleaner, rinsing in deionized H_2O in an ultrasonic cleaner, chemically cleaning in 4 parts HNO_3 to 1 part deionized water, rinsing in deionized water, and drying with oil-free and filtered N_2. The AES analysis of the surface conducted after the cleaning procedure closely resembles the spectrum of a sputter cleaned Ag surface. Small contaminant levels of S, Cl, C, and O were observed but the S, Cl, and C peaks were removed during the first few permeation runs of oxygen through the membrane [54], thus providing a clean Ag sample for experiments.

The grain growth of the Ag membranes was stabilized during the prerun vacuum degassing before oxygen was admitted to insure maximum growth of the grains. The grain size distribution varies from approximate diameters of 1 to 5 mm

with a mean diameter of about 1.1 mm. Grain densities determined by the linear intercept method were found to be 1.25 grains/mm^2. Some twinning also was observed. Details of these membranes have been reported previously [77].

Apparatus

The UHV permeation system (ultimate pressure less than 2 x 10^{-11} Torr) employed in this work was equipped with a main ion pump of 500 liters s^{-1}, a titanium sublimation pump, a quadrupole mass spectrometer (QMS), and ion gauges for signal detection. A small calibrated conductance f was used to separate the measurement chamber from the main ion pump in order to provide a known conductance limitation and therefore a known flow rate out of the measurement chamber. Measurement of the pressure, P(t), then allowed the determination of the permeation flux J(t). The high-pressure side of the membrane was also ion pumped to permit appropriate cleanup of the high-pressure side of the membrane surface and of the oxygen gas supply line.

The room temperature background gas spectra observed in the measurement chamber before and after introducing 100 Torr oxygen (into the high-pressure side of the system) were identical, thus indicating no leakage through the membrane. Eventually, however, the O_2 peak was observed and became the dominant signal as the Ag membrane was elevated in temperature.

A separate apparatus was used for an AES study of the large-grain Ag. The apparatus is described in detail in appendix 1. The AES data were taken using the CMA operated in the nonretarding mode with the coaxial electron gun operated at an energy of 3 keV. The CMA was also used to perform ion scattering spectroscopy (ISS). In ISS a primary beam of 1 keV He^+ ions at a flux of < 10 $\mu A/cm^2$ and a scattering angle of about 147° were used. The Ag sample was heated by electron bombardment using a tungsten filament place behind the sample.

Procedure

Permeation measurements

After vacuum degassing the membrane at 800 C, oxygen was admitted to the high-pressure side, equilibrium flow was established, and the upstream pressure was removed to determine the pressure decay in the measurement chamber. From the equilibrium pressure obtained for each run the permeability is computed from Eq. (7). After the high-pressure side is evacuated, a linear decay on a ln P(t) versus time plot is predicted by Eq. (12), from which the diffusivity can be determined. Figure 5 shows representative data for oxygen breakthrough to steady state (T_{Ag} = 550 C, P_o = 150 Torr O_2) and then pressure decay (T_{Ag} = 550 C, P_o -> 0 Torr O_2). After several cycles of this procedure to clean the membrane

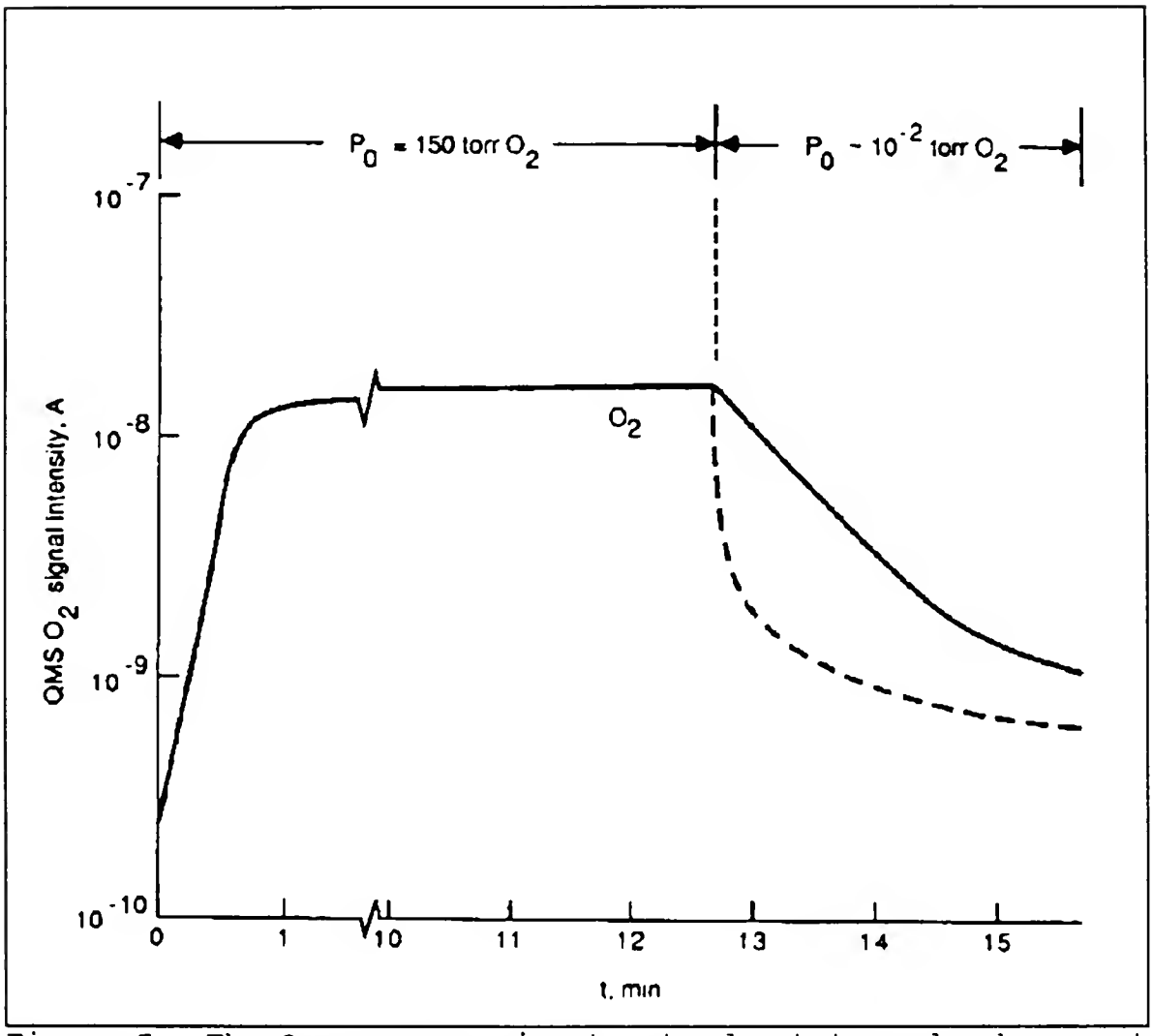

Figure 5. The O_2 pressure rise to steady state and subsequent pressure decay following pump down of upstream side. Dashed curve represents normal pump down without evolution of oxygen from the membrane.

on both faces, data were taken at 25°C increments over the temperature range of 400-800°C and over the high-side pressure range of 5-250 Torr by monitoring the signals of both the ion gauge and the QMS. The emission current of each instrument was maintained at low values (0.4 and 0.5 mA, respectively) to minimize instrument pumping.

The curvature that appears in Fig. 5 after the linear decay in the signal is due to a weak incorporation of oxygen into the stainless steel walls of the vacuum system. When the high-pressure side is evacuated, a linear decay occurs as predicted by Eq. (12); but ultimately, as the pressure descends toward the background level, the data begin to curve because the charged walls now see an opposite concentration gradient that causes oxygen to desorb back into the gas phase. The increase in oxygen gas flux results in an increased background pressure, but is substantially less than the gas flux evolving from the membrane immediately after the high-pressure side is evacuated, so it does not alter the linear decay necessary to determine the diffusivity. This effect has also been substantiated by separate experiment. Note the dashed line in Fig. 5 that represents the decay when the membrane is uncharged with oxygen and the system has been backfilled to the same O_2 pressure that occurs during permeation.

At the higher temperatures studied, the vapor pressure of

the Ag is sufficiently large to cause some material loss from the membrane. For example, at 800°C, the vapor pressure is approximately 5 x 10^{-5} Torr, which results in a sublimation rate of 0.01 mm/h. This represents a significant mass loss and required corrections for each experimental run.

The procedure described above was used to study five different Ag membranes from which consistent and reproducible results were obtained.

AES experiments

For the AES study an Ag membrane was prepared as previously described and then charged with oxygen at 100 Torr for 2 h at 500°C. The sample was then mounted in the UHV analytical system and sputtered until AES and ISS showed that the surface was clean. The sample was then heated by electron bombardment and the temperature was measured using a thermocouple spot welded to the edge of the Ag sample. Since the Ag membranes were thin and Ag has a high vapor pressure, it was difficult to heat the sample evenly above 500°C. Above this temperature much of the energy input to the sample caused vaporization of the Ag. Because the energy could not be evenly distributed in the thin membranes, a large temperature gradient (>350°C) across the sample was formed. The temperature at the edge of the sample was established at 600C, and the canter was near the melting point (960°C). The sample was then cooled to room temperature and studied with AES.

Results and Discussion

Permeation Measurements

The permeability data are presented in Fig. 6. The linearity is quite good and was repeated over six separate runs. Several initial runs were required, however, before the data became repeatable, presumably because of contaminant removal by the oxygen. An important feature of the permeation technique used in this work is that bulk cleanup of the material studied occurs more readily because very thin membranes (≈0.254 mm) were used. Segregation of the impurities to grain boundaries and then to the free surface can occur much faster, thus providing a more rapid cleanup by oxidation and desorption of reaction products. The mass spectra observed in the measurement chamber indicated a nominal fragmentation pattern for O_2 and showed even less contamination than the UHV work of Beavis [78]. The low levels of CO and CO_2 and the absence of other contaminants reflect a very clean membrane. A comparison with the apparent permeability determined by Eichenauer and Muller [3] (fig. 6) shows that the data reported here are lower in magnitude by a factor of 3.2 but similar in slope. One possible explanation for the lower magnitude is that the grain boundary diffusion component was minimized in this work due to the large grains. Silver is known to be sensitive to impurities

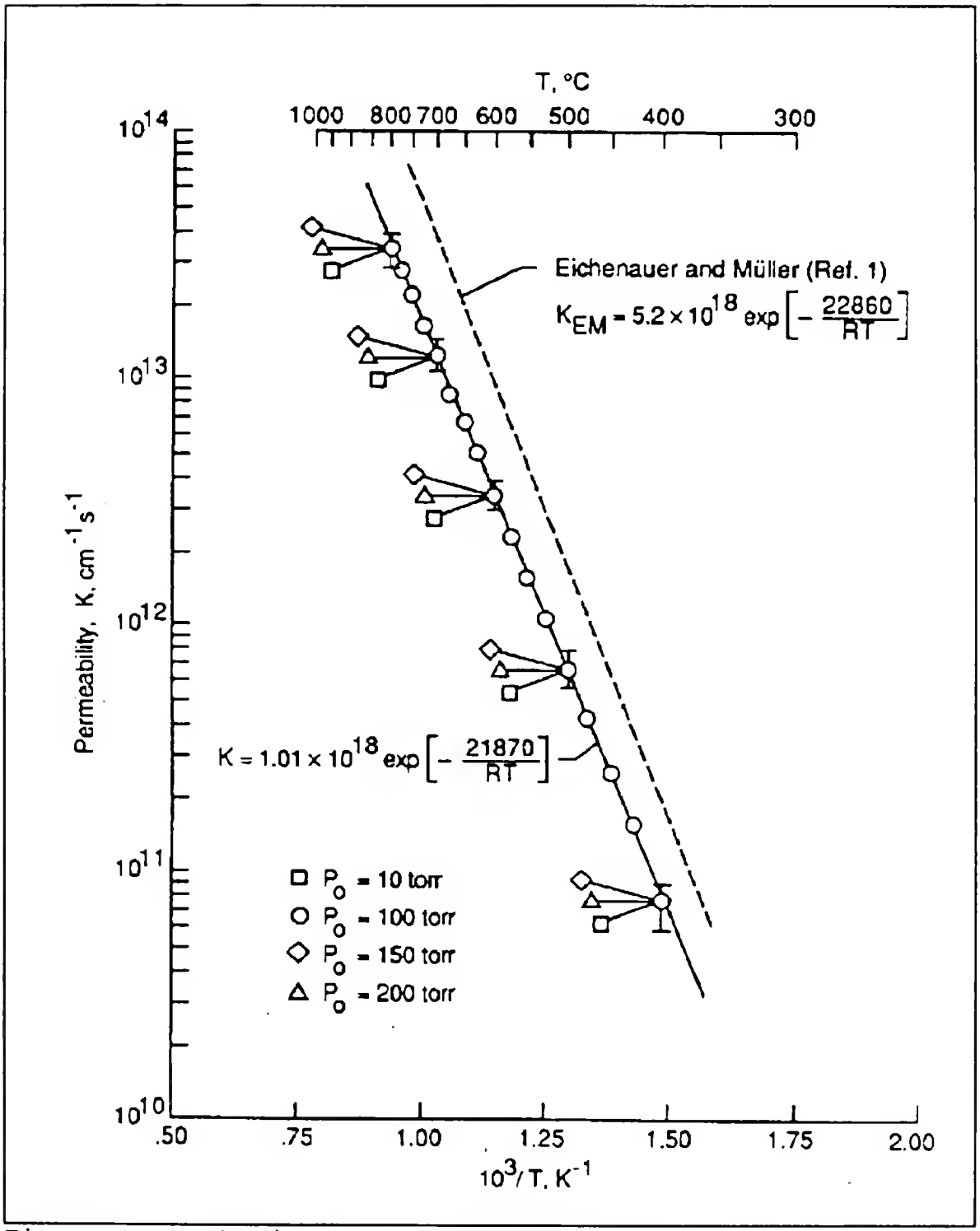

Figure 6. Arrhenius plot of oxygen permeability of the large-grain Ag compared to past research.

restricting grain growth since the segregation of the impurities to the grain boundaries tend to slow down or stop intergranular transfer of Ag atoms from smaller to larger grains. This suggests that more grain boundaries and therefore many more transport paths are present in less pure Ag. Unfortunately, there is virtually no information on the microstructure of the Ag samples used in the earlier studies, but they are probably small grain samples since the Ag was not high purity. The purest Ag studied by past researchers was reported by Eichenauer and Muller (99.99 % vacuum melted at an ultimate pressure of $\approx 10^{-3}$ Torr).

The permeability equation determined from a least-squares fit of the data presented here is

$$K = 1.01 \times 10^{18} \exp(-21870/RT)\, cm^{-1}s^{-1} . \quad (13)$$

The activation energy associated with these data compares well to that of Eichenauer and Muller (E_a = 22 860 cal/mol). It is important to note that all permeation data with upstream pressures of P_o = 10, 100, 150, and 200 Torr, plotted on the same straight line (fig. 6). This agrees with Sievert's Law and the assumption that the O atoms move through the Ag in the atomic state.

The diffusivity data showed some variation in the first few runs as the membrane became more and more contaminant free, but ultimately became very repeatable. As shown in Fig. 7, a break in linearity occurs in the diffusivity at $\approx 630^{\circ}C$.

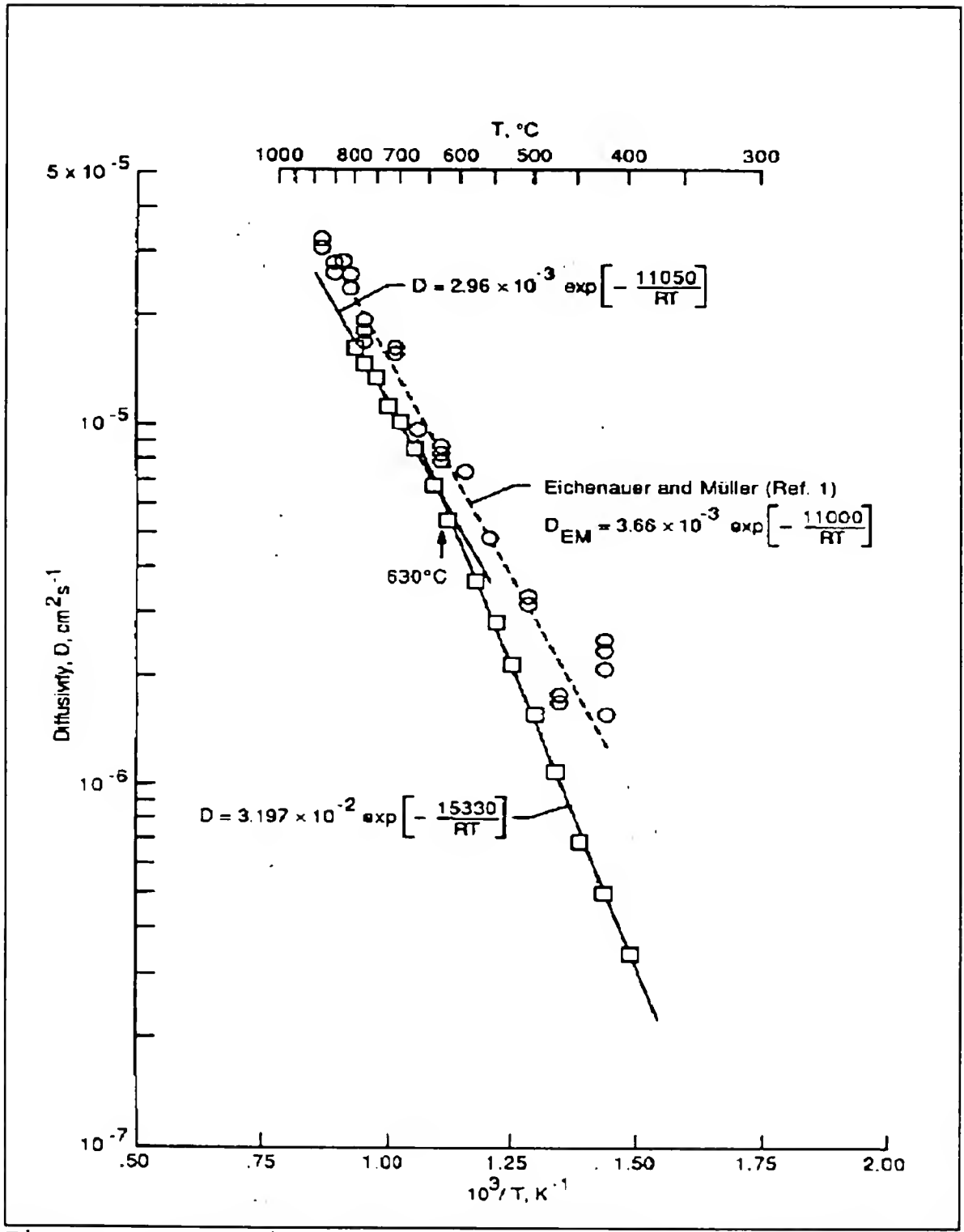

Figure 7. Arrhenius plot of oxygen diffusivity in Ag compared to past research. Note the diffusivity break in linearity at T = 630 C.

A break is commonly seen in systems where there is a transition from grain boundary diffusion to lattice diffusion with increasing temperature, but in all such cases the activation energy for lattice diffusion is greater. In this work the higher temperature regime has a lower activation energy. The equations determined from the diffusivity plots are

$$D = 2.96 \times 10^{-3} \exp(-11\ 050/RT)\,cm^2s^{-1}\ ,$$
$$630°C < T < 800°C, \qquad (14a)$$
$$D = 3.2 \times 10^{-2} \exp(-15\ 330/RT)\,cm^2s^{-1}\ ,$$
$$400°C < T < 630°C. \qquad (14b)$$

In the higher temperature range, the value of the activation energy (E_a = 11 050 cal/mol) is almost exactly that obtained by Eichenauer and Muller (E_a = 11 000 cal/mol). At temperatures below 630°C, however, the value of the activation energy (E_a = 15 330 cal/mol) is considerably higher.

In order to examine what occurs in the higher temperature regime, the desorption of oxygen from the membrane was studied. Figure 8 shows the desorption spectrum of O_2 from the membrane (vacuum on both sides) observed during the increase in membrane temperature to 800°C. Note that at 630C sufficient thermal energy exists so that the onset of vacuum desorption of oxygen from the membrane occurs. This indicates that the oxygen atoms are probably migrating with an increased mobility above this temperature. This increased mobility can

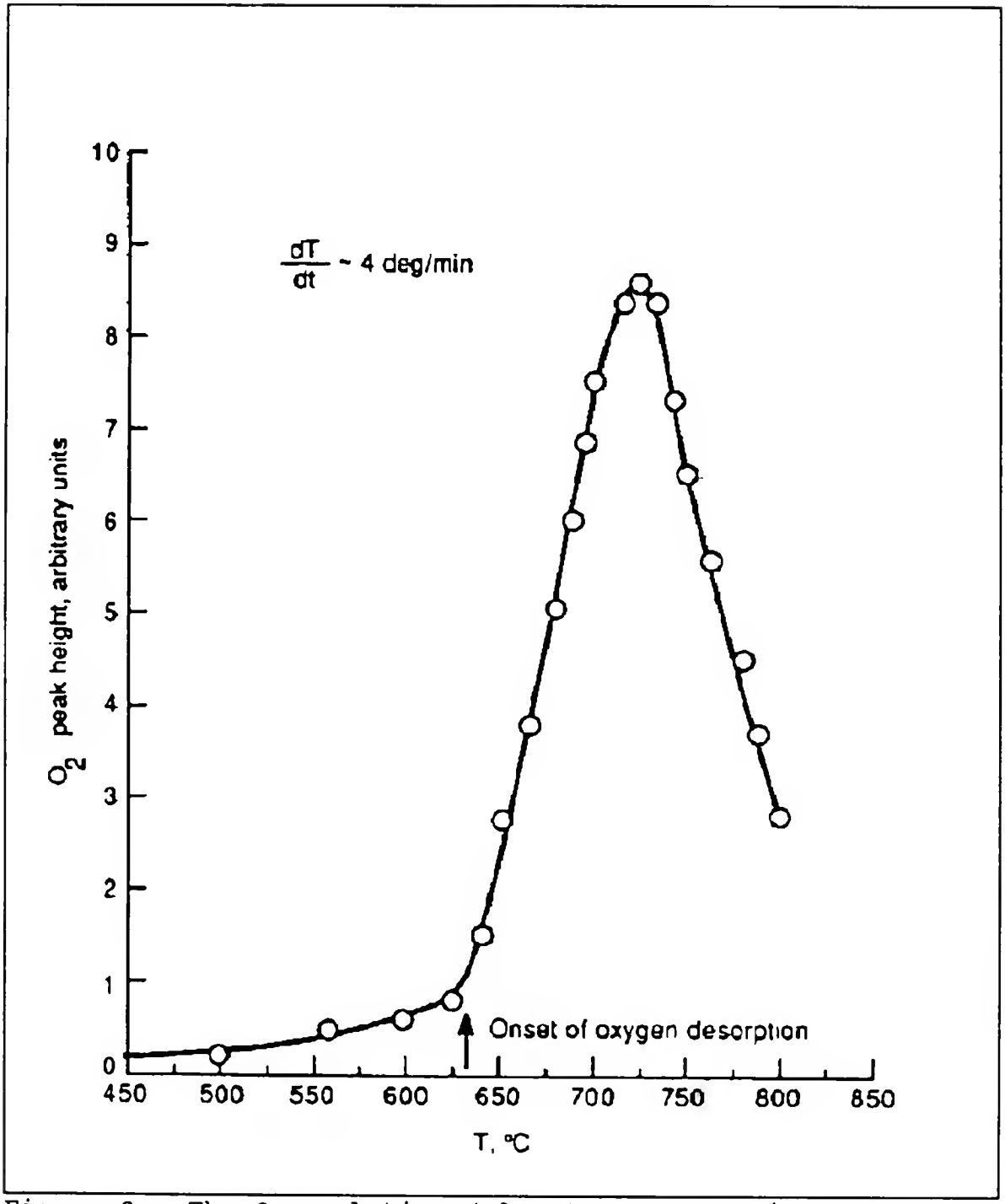

Figure 8. The O_2 evolution (slow temperature increase) from Ag membrane detected downstream when the upstream pressure is at $p = 10^{-8}$ Torr.

be correlated with the diffusivity data represented by Eq. (14a). In terms of diffusivity, whatever differences that exist between the microstructure and the purity of our Ag compared to that of Eichenauer and Muller must have been overcome by the thermal energy, since the diffusivity values are the same. In the low-temperature regime, the larger activation energy and the lower mobility indicate a different control of oxygen atom transport, possibly trapping. Mitchell et al.[79] have examined the trapping effects of hydrogen in copper due to the addition of substitutional impurities Er, Zr, and Ti. They found no change in the permeability of to 4 at. % of Zr, but they did observe a significant decrease in the magnitude of the effective diffusivity (D_{eff} represents the effect of the trap in contrast to the D in pure Cu). Furthermore, the slope of the D_{eff} (for all impurities) in an Arrhenius plot was also significantly greater than for the D in the pure Cu and represents an increased activation energy because of the traps. According to the analysis of Mitchell et al., the observed activation energy E is the sum of the trap energy E_T and the activation energy E_a. The trap energy E_T for this work is 4280 cal/mol. Johnson and Lin have observed a diffusivity break similar to that observed in this work for the system H/Fe [80]. They attribute the higher activation energy in the lower temperature range to the higher efficiency of traps, which, in their case, were vacancies.

In this study of high-purity Ag, vacancies and interstitial impurities are more likely to be trapping centers than are substitutional impurities. The vacancy concentration in Ag ($E_f \approx 25.3$ kcal/mol) is about 4×10^{17} cm^{-3} at 800°C, but these vacancies could be filled by oxygen atoms at elevated temperature that would then stabilize them in the low-temperature regime.

Lattice diffusion is the dominant mechanism in this work because of the very large grains, but grain-boundary self-diffusion is well known to occur in Ag and predominates over lattice diffusion below 750°C for small grain material [81]. Therefore, the diffusion of oxygen in the grain boundaries might also be quite significant since oxygen is a smaller atom than Ag and has less chemical affinity for Ag than Ag has for itself. For these reasons, grain boundary diffusion of oxygen was likely to have been a significant component in past research where the Ag grain size was small.

AES experiments

Folowing the heat treatment of the Ag sample, AES line scans of the O and Ag peaks were taken at room temperature and found to be quite repeatable (see Fig. 9). These scans were obtained by slowly moving the 1.0 μm primary electron beam from the center of the sample to the edge of the sample. Several interesting features are revealed by this reproducible line scan. First, essentially no oxygen is present near the

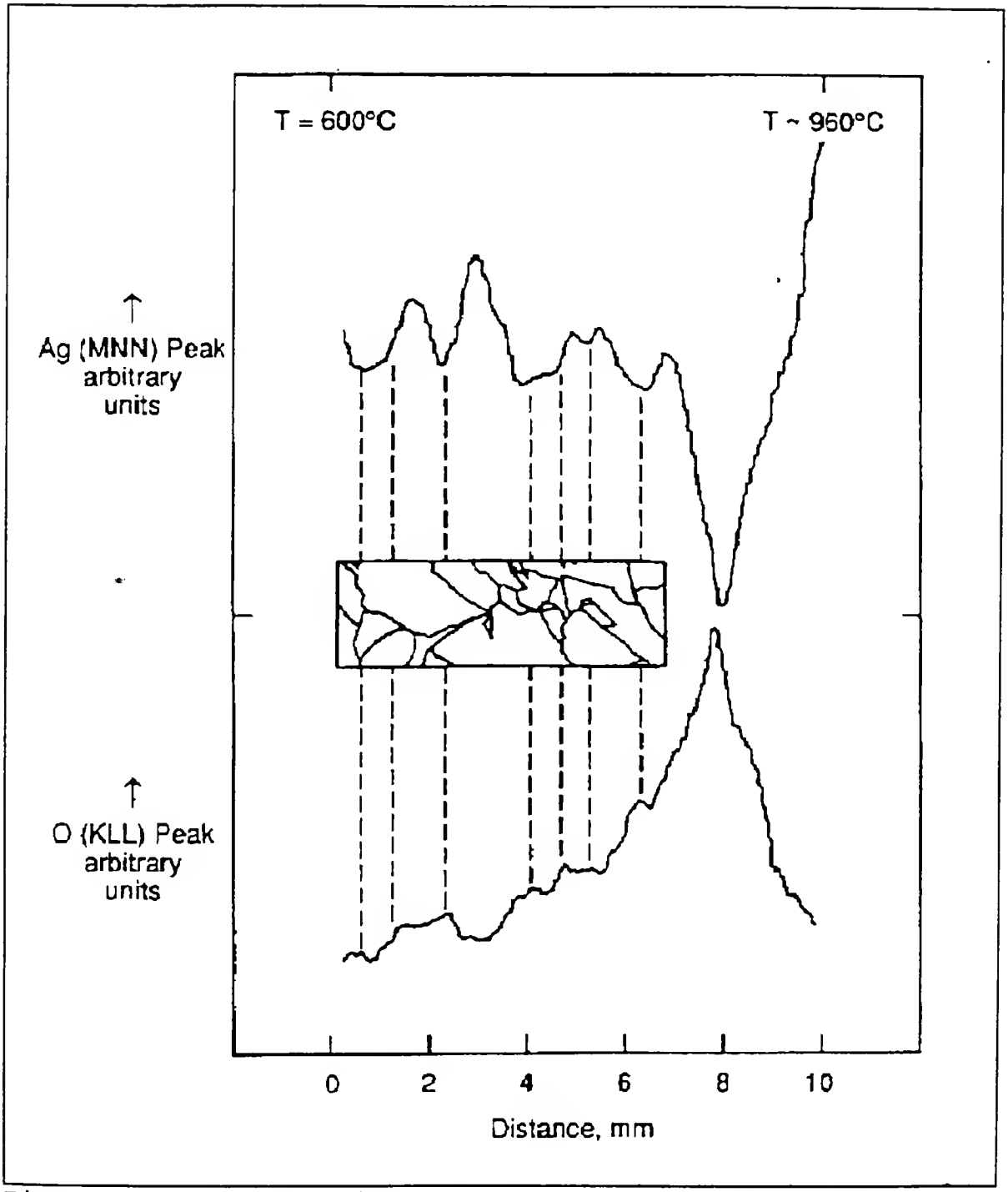

Figure 9. The AES line scans from the sample edge to the center of the Ag membrane. The insert in the center is a trace of the Ag membrane grain boundaries.

region where the sample was near the melting point (10 mm) from the edge of the disk). This implies that the oxygen either desorbed or moved to a cooler portion of the sample. The region between 7 and 9 mm from the edge of the sample contains the largest amount of surface oxygen. This region was hot enough for the oxyegn to be driven to the surface from the bulk Ag but not so hot that it desorbed or migrated away from the region. An AES sepctrum taken from the region where the oxygen signal is a maximum shows only a very small amount of oxygen (as indicated by the O/Ag ratio of less than 6%). Moving the electron beam from 7 mm to the edge of the sample results in a decreasing oxygen signal. This is due to a decreasing temperature across the sample which results in less oxygen migrating to the surface. The structure that is particularly apparent in the Ag peak height line scan is due to the presence of grains and grain boundaries. Microstructure measurements show an average grain size of about 1.25 mm, which corresponds well with the average distance between the observed Ag minima and O maxima. The insert in Fig. 9 is an outline of the grain boundaries from a micrograph of the Ag. Note that the Ag peaks and O valleys are about the same distance apart as the average grain size.

Past research in the surface properties for the O/Ag system shows a very small sticking coefficient and virtually no adsorption on the (100) and (111) planes and only about 5%

on the (110) plane [39,41]. This indicates little oxygen affinity for adsorption on single crystal Ag and suggests a barrier to oxygen dissolution into the bulk. In this work we have observed a very small oxygen AES signal in the middle of the grains of oxygen-charged Ag but have observed a much larger signal at the grain boundaries. Further, as the sample was heated to above 600°C, intragranular oxygen signals became more detectable, but the signals at the grain boundaries dramatically increased, suggesting rapid segregation to the grain boundaries and ultimately to the free surface.

Summary

We have determined the permeability and diffusivity of oxygen through high-purity large-grain Ag. The magnitude of the permeability found in this work compared with past research is lower by a factor of 3.2. The diffusivity curve shows two linear regimes. The high-temperature regime agrees very well with past research, but the low-temperature regime has a higher activation energy, probably due to trapping. The AES experiments indicate there is a much smaller intragranular oxygen signal intensity compared to that observed at the grain boundaries and that this difference is further accentuated with increasing temperature. Although lattice diffusion is the dominant mechanism in this work, the permeability comparisons, the AES results, and the implications of past research strongly indicate the importance of grain boundaries

in the O/Ag system. The study of oxygen through fine-grained Ag (Ag 0.5% Zr) and Ag single crystals will ultimately provide more definitive answers to this question.

A NONDESTRUCTIVE DEPTH PROFILE STUDY OF OXYGEN-EXPOSED LARGE GRAIN SILVER USING ARAES AND ISS

Introduction

In the previous chapter, evidence that the transport properties of oxygen through polycrystalline silver are influenced heavily by defects and grain boundaries is given. In addition, some knowlege of the position of the oxygen in relation to the surface is desired in order understand any possible mechanisms for transport and ESD of oxygen.

Several studies of single crystal Ag(110) have indicated that a subsurface oxygen species might be formed under certain conditions. Segeth, Wijngaard, and Sawatzky [82] recently found evidence using angle resolved ultraviolet photoelectron spectroscopy (UPS) that a surface relaxation can occur on oxygen exposed Ag(110). In addition, Kuk and Feldman [83] have found using high energy ion scattering spectroscopy (HEISS) that Ag(110) undergoes a multilayer surface relaxation the first two layers are contracted and the second two layers are expanded relative to the bulk. Backx et. al. [49] have suggested that a subsurface oxygen species is formed by oxygen exposure of Ag(110) which can be transferred to the surface

by heating to 200°C. It is likely that the subsurface oxygen which has been observed is located in the subsurface region in which the lattice spacing is expanded relative to the bulk.

These studies indicate that at least some of the surfaces exposed in a polycrystalline sample might undergo relaxation and that their interaction with oxygen may not be a straightforward surface adsorption and bulk diffusion. In this study large-grain, high-purity silver was exposed to oxygen and analyzed using ion scattering spectroscopy (ISS) and angle resolved Auger electron spectroscopy (ARAES) [84]. By combining these techniques, a non-destructive depth profile of the near surface region can be obtained, and that information used to elucidate a schematic oxygen potential distribution as a function of depth for the first few atomic layers.

Experimental

The sample used in this study was vacuum melted high purity (99.999%) silver with an average grain size of about 1 mm. The sample was solvent cleaned in a manner similar to that discussed previously. Residual contaminants were removed in the analysis chamber by repeated heating to 500°C and Ar sputtering. Oxygen doses were performed in a preparation chamber attached to the main analysis chamber. Doses were performed at 75, 150, 200, and 250°C in 75 Torr of oxygen. The sample heater was designed with the hot filament protected

from oxygen exposure so that the high pressure doses could be achieved.

Energy analysis was performed using a Perkin Elmer PHI model 25-270AR double pass cylindrical mirror analyzer equipped with an angle-resolving aperture. ISS and ARAES data were taken in the non-retarding mode. ISS data were generated by using 1 keV He^+ ions and a defocused ion beam in order to minimize damage. Scattering angles of 144° and 64° were used for ISS. Standard backscattered (144°) ISS data were obtained for oxygen quantification, but backscattered ISS proved to be insensitive to trace quantities of low molecular weight impurities so forward scattered (64°) was used to determine sample cleanliness (Fig. 10). From the data presented in figure 10, it is estimated that the sensitivity of forward scattered ISS to surface oxygen is about 1000 times higher than that for backscattered ISS. It should be noted that although a silver surface can appear clean by backscattered ISS, the forward scattered ISS reveals several surface contaminants. Although these contaminants are present at low levels, the behavior of silver towards oxygen is drastically changed by very small levels of contaminants since most contaminants bind oxygen much more strongly than does the silver.

AES data were obtained by using the coaxial electron gun operated at 3 keV. Detection of the Auger electrons was

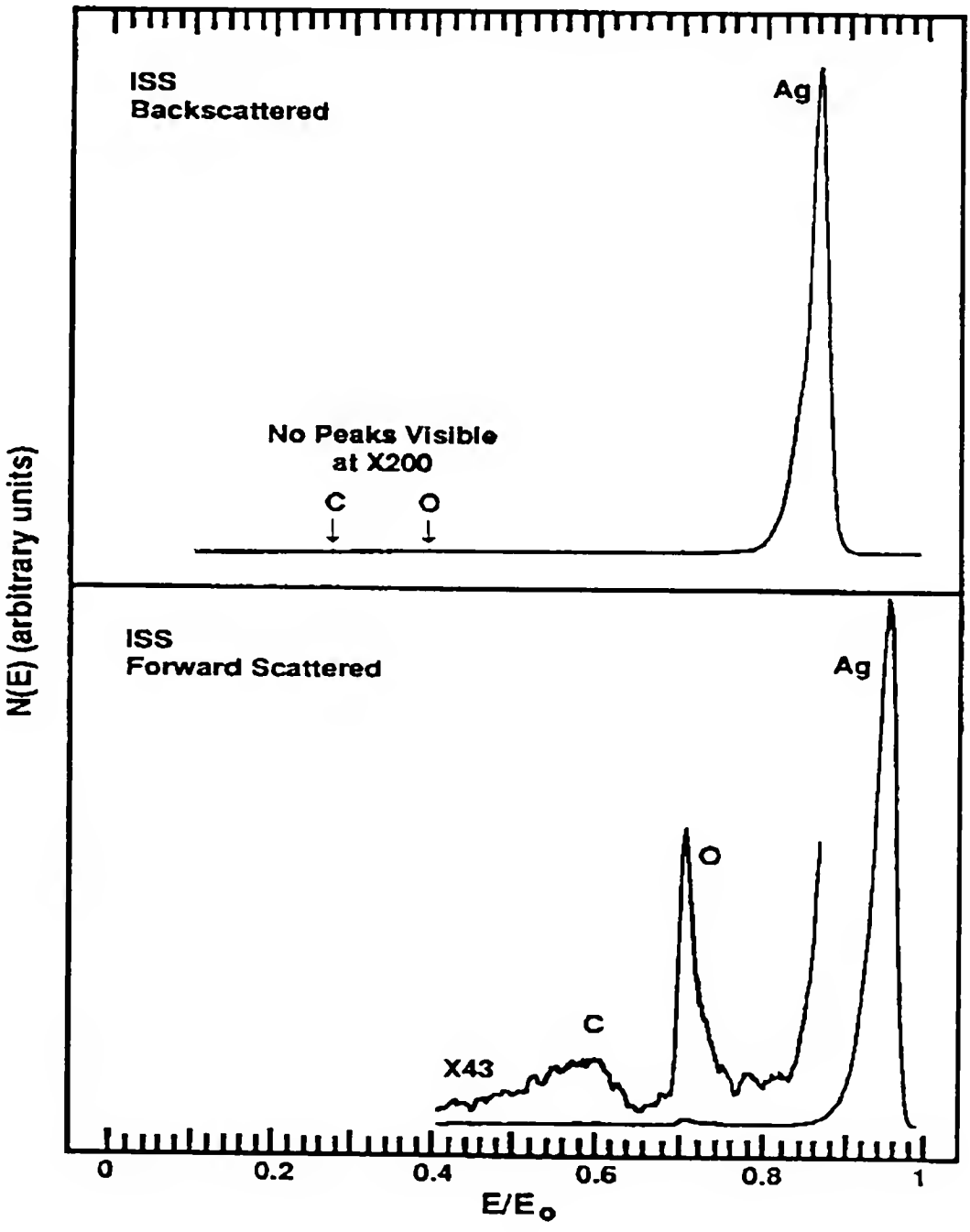

Figure 10. Comparison of forward scattered and backscattered ISS data for the same sample. Note the contaminants which are evident in the forward scattered spectrum are not detectable in the backscattered ISS spectrum.

performed using a lock-in amplifier with a peak-to-peak modulation of 0.5V in the outer cylinder. AES data were obtained with the sample surface normal to the electron beam and the electrons emitted in a cone approximately 42° about the normal were collected. In ARAES, the sample is tilted so that the electron beam strikes the sample at 20° from the surface and the a 90° angle resolving aperture is positioned such that only electrons emitted at an angle of about 20° from the surface are collected. The technique has been described in detail elsewhere [84].

The information obtained in the techniques of ISS, AES, and ARAES can be combined to give a semiquantitative depth profile of the surface region. It is known that ISS is sensitive to only the first monolayer since ions which penetrate beneath the surface have a nearly 100% chance of being neutralized or undergoing multiple scatterings and simply contributing to the "inelastic background" and not to the elastic peaks which are the basis for quantification [85,86]. AES, however, is sensitive to about 30 atomic layers as shown in fig. 11a. The data presented in Fig. 11 is calculated based on the mean free paths of the incoming and the emitted electrons. The mean free path of both the incident and emmitted electrons was assumed to be 10 Angstroms [88] and the lattice constant used was that determined by Kuk and Feldman for the Ag(110) surface [83]. The mean free path

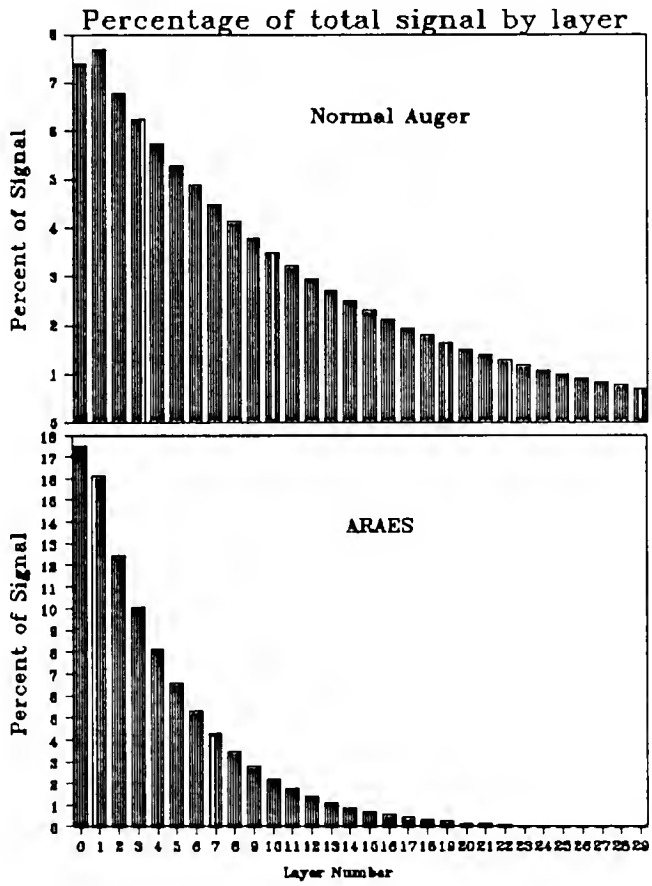

Figure 11. Results of the calculation of depth sensitivity of AES and ARAES as a function of the silver layer number.

data measured thus far show a scatter of several Angstroms in both the primary electron and Auger electron energy ranges so the results of the calculations presented, while correct in relative magnitude of AES and ARAES signals, should be considered approximate. It should also be noted that the calculation considers only the angular dependence of the mean free path and not the energy dependence. In addition, a surface relaxation was assumed to take place and was also modeled after the findings of Kuk and Feldman [83] for the Ag(110) surface. The assumption of a surface relaxation in the polycrystalline sample is justified based on the findings of this work. The calculated depth sensitivity of the ARAES data is given in figure 11b. Notice that the sensitivity of the ARAES is much greater near the surface than AES and that ARAES is sensitive only to about 15 atomic layers.

Results and Discussion

Determination of Relative ISS Cross Section

In order to quantify ISS data it is generally necessary to experimentally measure the relative ISS sensitivities of the species involved. Theoretical calculations are unreliable since they depend strongly on the model chosen for the interaction potential between the ion and the target atom [89]. In addition, ion neutralization probabilities can differ between target elements and this aspect of the cross section is also very difficult to model.

The detected ISS N_i signal can be approximated by [85]

$$N_i = K\ S_i\ C_i$$

where

K = a factor which depends on the primary flux, instrument transmission, and other factors which don't vary between target elements

S_i = the elemental sensitivity

C_i = the concentration of species i at the surface

If we assume that the total density of atoms on the surface doesn't change with coverage, then for a binary system (O adsorbed on Ag) it can be shown that for any two different coverages

$$(N_{O1} - N_{O2}) \ / \ (N_{Ag2} - N_{Ag1}) = S_O \ / \ S_{Ag}$$

In order to determine the relative sensitivity, a silver sample was cleaned and dosed with oxygen. Several ISS spectra were then obtained during sputtering. Since the oxygen is sputtered preferentially, ISS spectra of varying surface oxygen coverages were obtained. The differences in oxygen signal were then plotted vs. differences in silver signal for all possible combinations of spectra obtained (fig. 12). The slope of the best fit line was determined to be 0.045 and represents the relative ISS sensitivity of O to Ag.

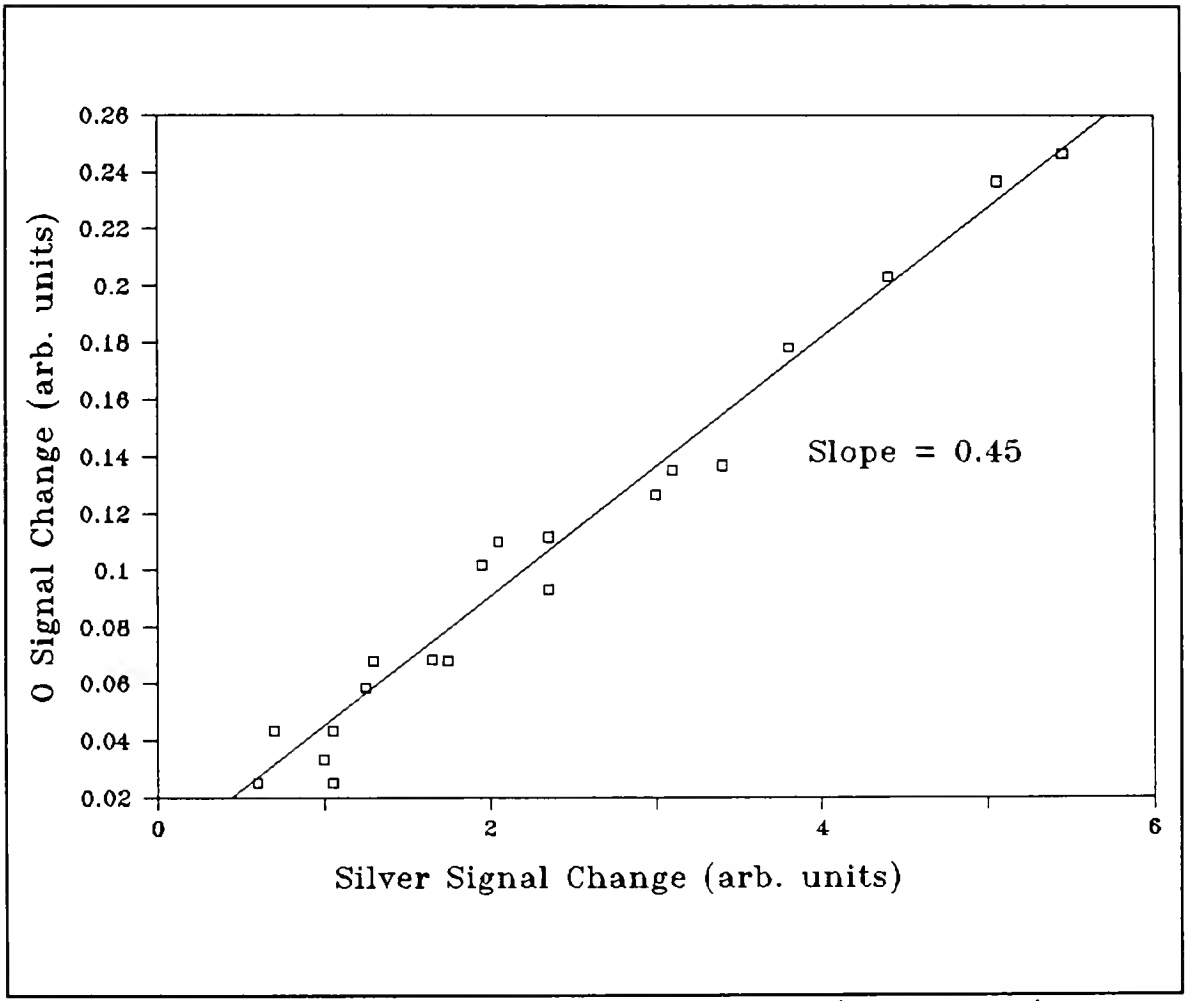

Figure 12. Plot of data used to find relative ISS sensitivities for a binary system. The relative sensitivity is given by the slope.

Oxygen Dosing Results

The ISS data as a function of dosing temperature for a pressure of 75 Torr are shown in fig. 13. The "clean" Ag surface shows no ISS oxygen signal. The rest of the ISS data show a rise in the oxygen surface concentration with increasing dosing temperature up to a maximum of about 50% of a monolayer. The normal AES data are shown in fig. 14. Like the ISS data, the "clean" silver shows no detectable oxygen signal greater than the noise level. However, as the dosing temperature increases, the normal AES signal saturates at an oxygen concentration of about 14 at. %. The ARAES data are given in fig. 15. Unlike either the ISS or AES data for the "clean" sample, the ARAES data show a detectable oxygen signal corresponding to 3 at. % oxygen. Much like the AES data the ARAES data also show that the silver saturates at an oxygen concentration of about 14 at. %. The oxygen concentrations calculated for all of the dosing temperatures and the "clean" sample are summarized in fig. 16 and are discussed in detail below.

The results for the clean sample seem quite unusual. The ISS data show clearly that the surface is free of oxygen, and the AES data show the surface region is apparently free of oxygen, but the ARAES data show that there is a small amount of oxygen present. ARAES is normally sensitive to the

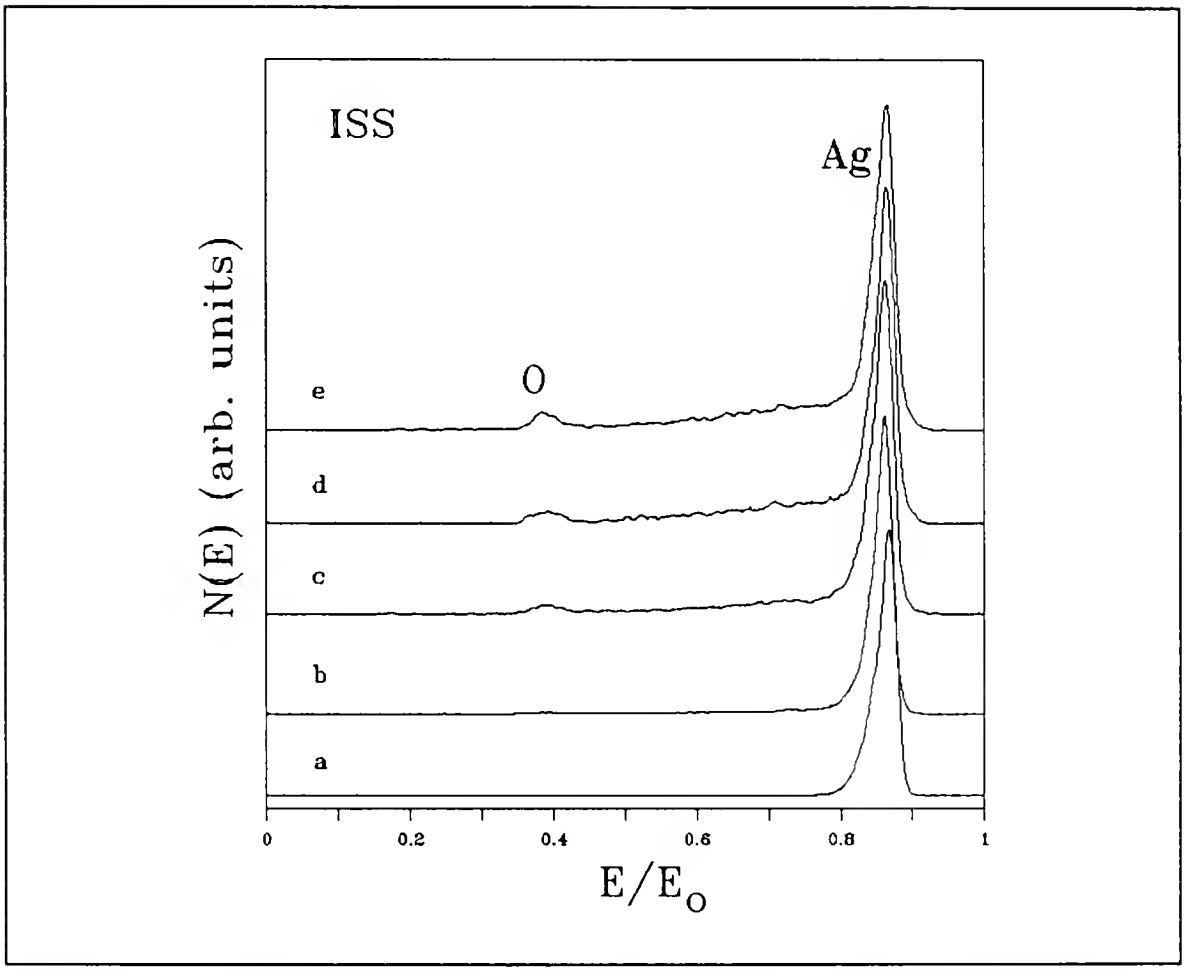

Figure 13. ISS spectra for the various dosing temperatures. a) "clean"; b) 75°C; c) 150°C; d) 200°C; e) 250°C

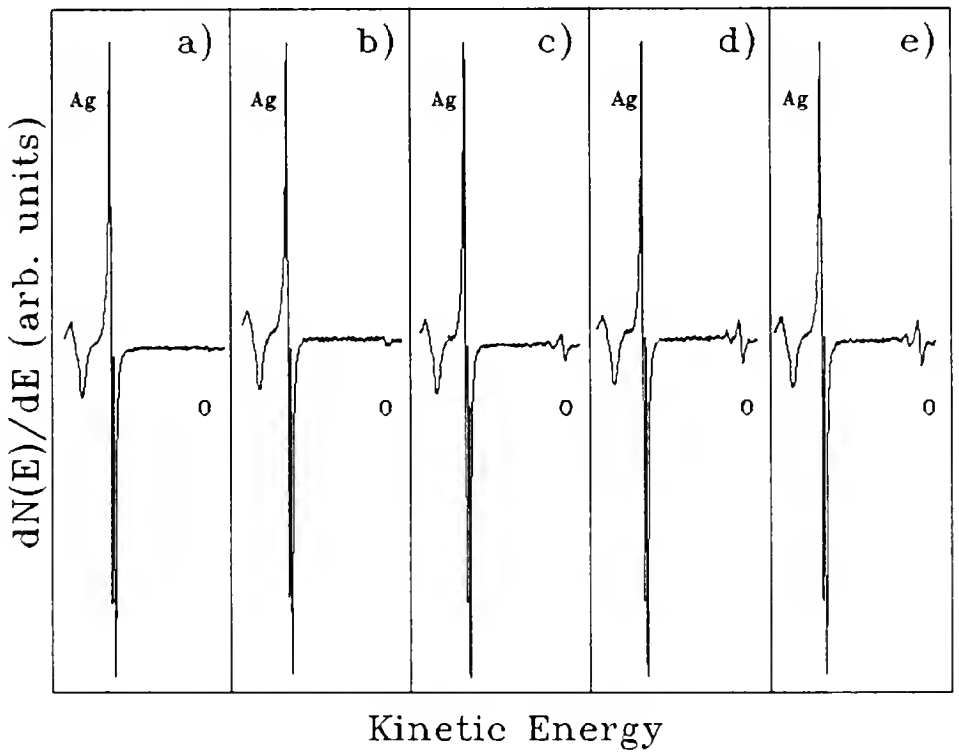

Figure 14. Normal (bulk sensitive) AES data for the various dosing temperatures. a) "clean"; b) 75°C; c) 150°C; d) 200°C; e) 250°C

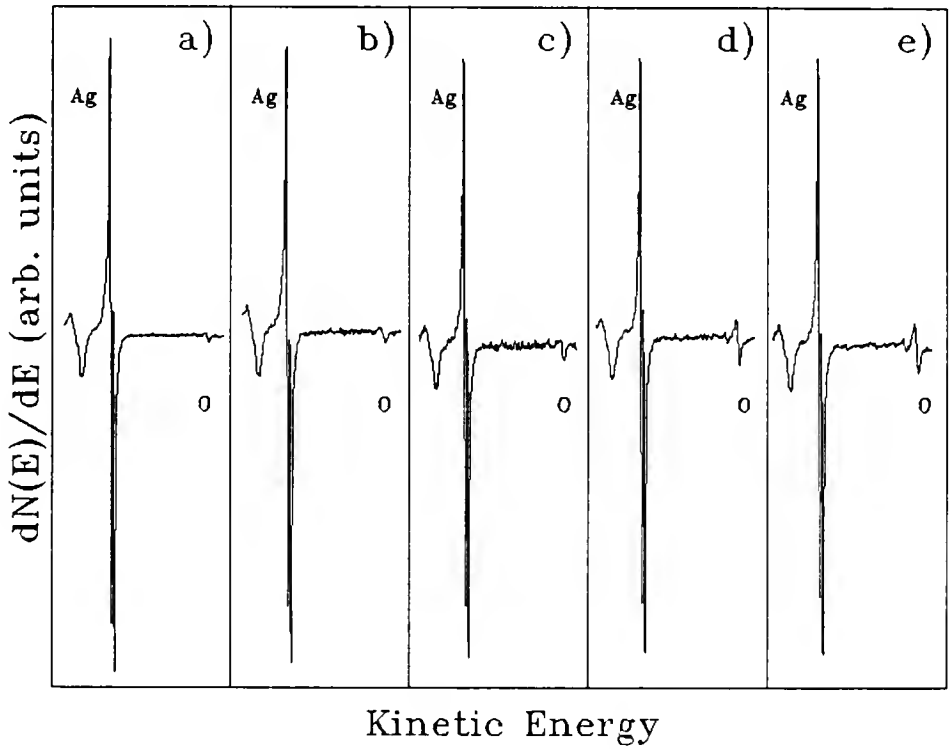

Figure 15. ARAES (near surface sensitive) data as a function of dosing temperature. a) "clean"; b) 75°C; c) 150°C; d) 200°C; e) 250°C

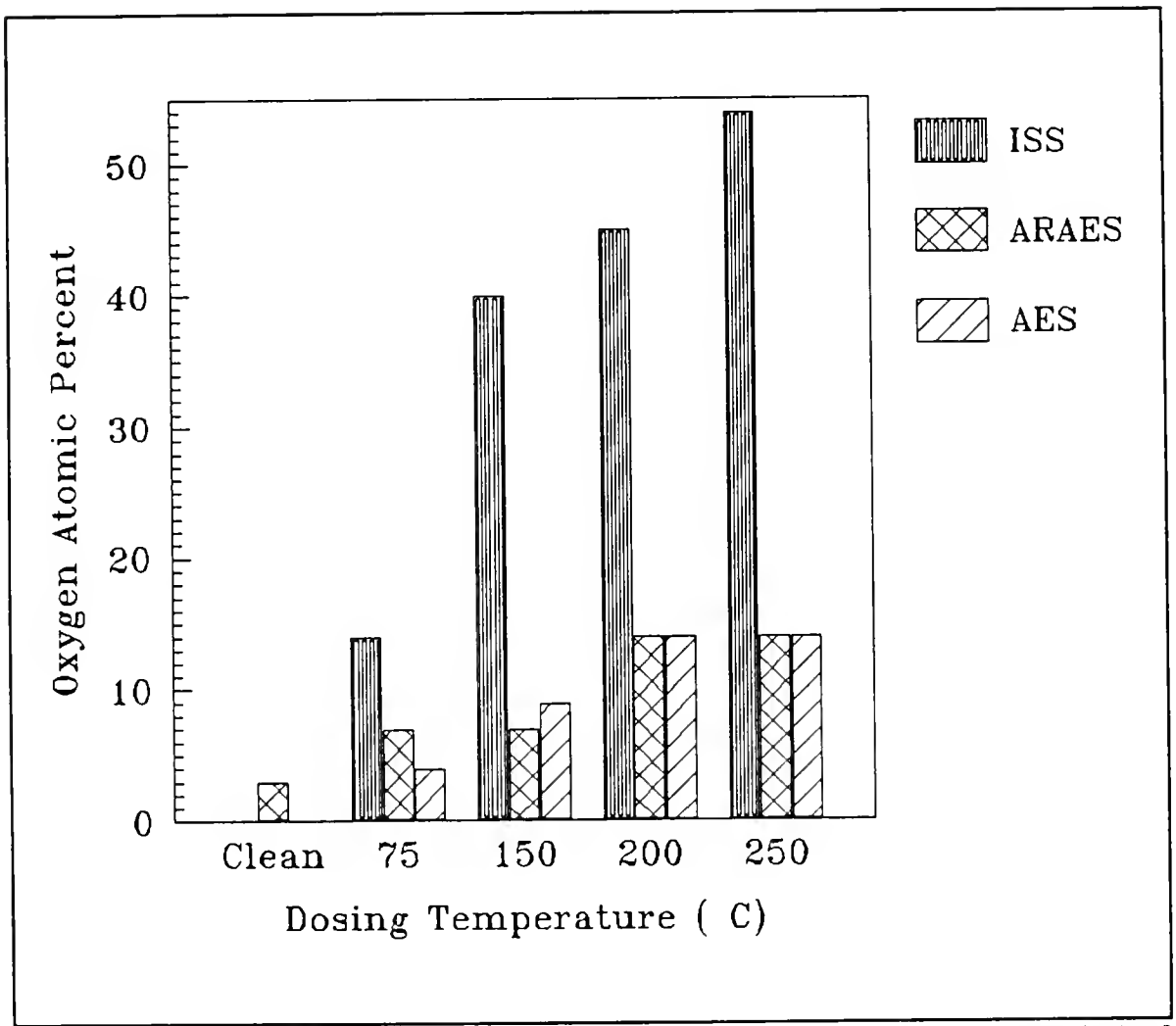

Figure 16. Summary of the atomic concentration calculated from the ISS, AES, and ARAES data for all of the dosing temperatures.

near surface region, however, in this case, ISS data show conclusively that there is no surface oxygen. The results can be explained by considering the relative sensitivity as a function of depth between normal AES and ARAES (fig. 11). The percentage of total signal for the first 4 layers in ARAES is about double that for normal AES in the same region. If the oxygen detected in the ARAES spectrum resided between the first and fourth Ag layers in small quantities (<5%) then it is possible that the oxygen signal would be below the normal limit of detectability of the normal AES of about 1%. It is reasonable to expect that the oxygen might be found exclusively in a subsurface region if the surface undergoes a relaxation in which one of the silver layers expanded relative to the bulk. If this were the case, the oxygen would have a lower energy in this region and would preferentially fill the expanded region.

After a 75 °C oxygen dose, the surface concentration of oxygen increases to 14% as indicated by ISS and the ARAES data show about 7% oxygen. The fact that the surface oxygen concentration increases faster than the near subsurface oxygen concentration indicates that the potential barrier to surface adsorption is lower than that for the oxygen to diffuse into the near surface region. The normal AES data indicate an oxygen concentration lower than that given by the ARAES data. This is due to the oxygen not yet diffusing a great distance

into the bulk. Since a large portion of the normal AES signal comes from depths beyond 5 atomic layers where the oxygen has not yet diffused, the oxygen concentration given by the total normal AES oxygen signal is lower than that given by ARAES.

After the 150 °C dose the surface concentration increases to 40% oxygen and the AES data show an oxygen concentration increase to 9% while the ARAES data indicate that the oxygen content remains the same at 7%. Given that there is a subsurface region in which the oxygen preferentially resides, the ARAES data seem to be inconsistent. Since the surface concentration increases it would be expected that the ARAES data would show a larger oxygen concentration than the normal AES data. The only way to explain this apparent discrepancy is by postulating that part of the surface relaxation involves the first two Ag layers which contract relative to the bulk and, therefore, increases the potential energy of the oxygen in that region. This suggests that the first layer below the surface is comparatively depleted of oxygen.

Dosing temperatures of 200 °C and 250 °C saturate the near surface region at about 14 at.%. Dosing at temperature up to 600°C and 100 Torr resulted in the same oxygen concentration as measured by AES. Both the normal AES and ARAES data indicate this concentration while the ISS data show an oxygen concentration of 50 at. %. The fact that the ISS give a high oxygen concentration while ARAES and normal AES give the same

lower oxygen concentration supports the hypothesis that a layer near the surface is oxygen deficient.

A schematic model of the potential variation and final oxygen concentration distribution as a function of depth which is consistent with the data is given in fig. 17. The fact that surface oxygen binds in relatively large quantities at low temperature doses indicates a low activation energy for surface adsorption but the relatively slow rate of movement of oxygen into the subsurface and bulk regions indicates an activation energy barrier between the surface and the bulk which is significantly higher than that for surface adsorption. The ARAES data for the "clean" sample indicate that there is a subsurface region in which the oxygen potential barrier to diffusion is significantly lower than in the bulk. In addition, comparison of the data at higher temperatures indicates that there is a layer in which the oxygen potential is increased relative to the bulk. Analysis of the relative depth sensitivities of ARAES and normal AES indicates that these layers are in the first four atomic layers of the Ag. Beyond the first few layers the potential can be expected to be some uniform bulk value between layers with some activation energy to go between layers. The model proposed is consistent with a surface relaxation consisting of a contraction relative to the bulk between the first two

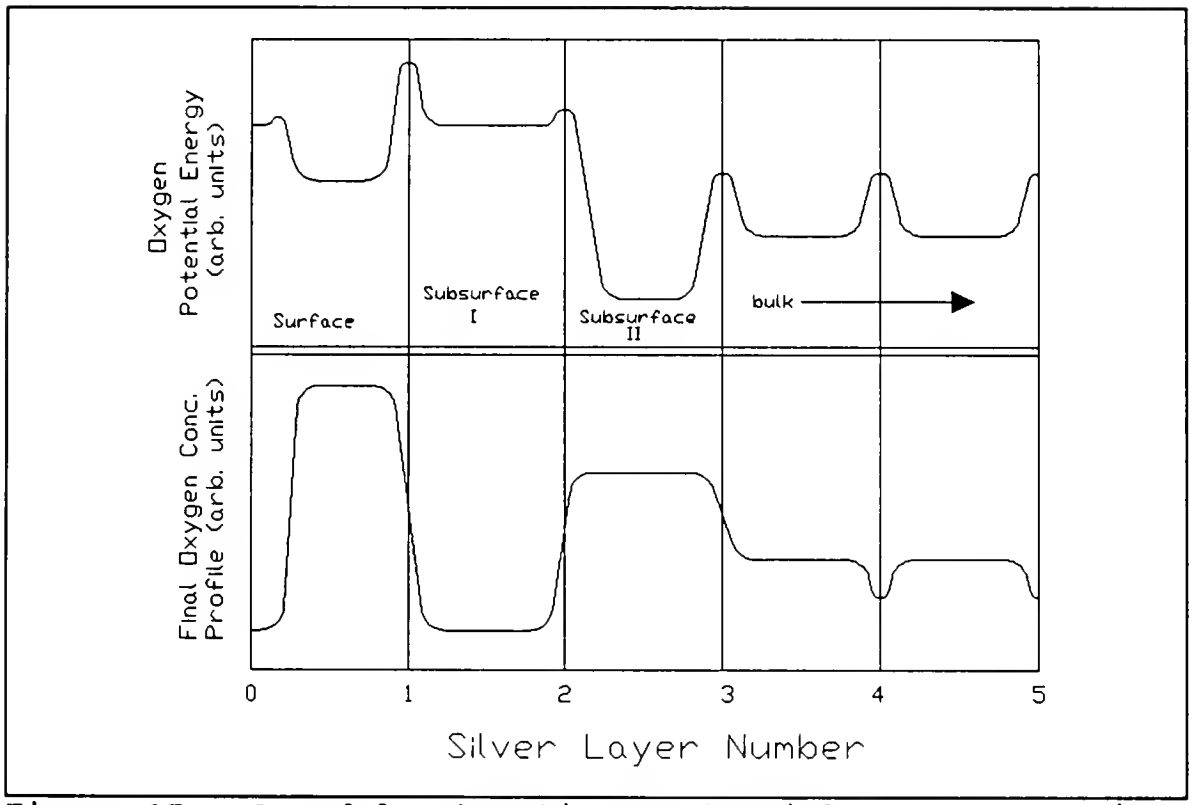

Figure 17. A model schematic O potential energy and final concentration profile which is suggested by the data presented.

silver layers and an expansion relative to the bulk between the second and third silver layers.

Conclusions

ISS, AES and ARAES are useful together as a semi-quantitative depth profile of the near surface region. For the oxygen exposed large-grain polycrystalline silver, evidence has been found for two subsurface regions with differing oxygen affinities. In one region, oxygen adsorption is enhanced relative to the bulk and, in the second, oxygen adsorption is reduced relative to the bulk. In addition, the oxygen adsorbs relatively easily on the surface, but diffuses more slowly into the bulk, indicating that the activation energy for adsorption is lower than the activation energy for bulk diffusion.

ESD AND SURFACE ANALYSIS STUDIES OF SILVER/0.5% ZIRCONIUM ALLOY

Introduction

In order for a successful HOAG to be constructed, a relatively large increase in oxygen atom flux over that found in the transient experiments is required. The two factors limiting the flux are transport rate and ESD cross section. The data presented in chapter 2 suggest that grain boundary density can have an effect on oxygen transport rates through silver metal. These results suggest that increasing grain boundary density can increase the transport rates through the metal. In addition, a higher ESD yield is desired, either through an increased ESD cross section or an increased oxygen concentration on the surface.

A search of the literature provided no references to solid metals which had a higher permeability for oxygen at practical temperatures than that which was measured for the pure silver. However, it is known that small amounts of impurities in the silver can decrease the grain size, thereby increasing the grain boundary density. If the preferred transport mechanism for the oxygen through the silver is

through the grain boundaries, then the increased grain boundary density would increase the transport rates.

In addition to an increased oxygen transport rate through the membrane, an increased ESD cross section is desired. In his review of ESD phenomena[6], Hoflund stated that the desorbing particle flux can be written as

$$i_p = i_p\ (E_e, Q_e, \emptyset_e, \Omega_e, E_p, \emptyset_p, \Omega_p, \ , T, t, f(r))$$

where

E_e is the electron energy

Q_e is the electron flux

$\emptyset_e, \Omega_e$ are the polar and azimuthal angles of incidence

E_p is the desorbing particle energy

$\emptyset_e, \Omega_e$ are the polar and azimuthal angles of desorption

is the surface coverage

T is the temperature

t is the time of exposure to the electron beam

f(r) is the defect density function

For the polycrytalline case the azimuthal angles are not expected to play a role if the grain orientation is sufficiently random but all of the other factors can be important. Due to the difficulty of performing repetitive ESD experiments, very little is known about the effects which variation of these parameters on the ESD yield. In particular, very little is known about the effect of electron incidence angle on the ESD cross section. In order to

maximize the ESD cross section, the effect of the primary beam angle is examined in this study.

The Ag/0.5% Zr system was chosen for several reasons. The first, as mentioned before, is that grain growth in silver is inhibited by additions of small amounts of impurities such as zirconium. The addition of the zirconium tends to stop the intergranular transfer of silver from smaller grains to larger, thereby increasing the grain boundary density. The second reason for choosing zirconium is that it is readily oxidized to ZrO_2. If the Zr in the alloy segregates to the surface and oxidizes, it would cause an increase in surface oxygen concentration which would cause an increase in the oxygen ESD flux from the surface. The last reason for using Zr as the additive is that it forms a maximal valency oxide. It is theorized that ESD cross sections for ESD which occurs by the KF mechanism are maximized for maximal valency oxides. The KF mechanism depends on an interatomic Auger transition which involves valence electrons from the oxygen atom relaxing into a core hole on the metal atom. A relaxation involving intra-atomic valence electrons is much more probable than the interatomic transition if the valence electrons are available. Since the metal atoms of maximal valency oxides have their valence electrons used in the bonding orbitals, an interatomic transition is more likely than if the metal atom has one or more available valence electrons.

Another parameter which is of interest in the design of the HOAG is the ratio of neutral atoms to ions produced. As discussed in the introduction, the ratio predicted can vary greatly depending on the mechanism. Experimentally measured values reported in the literature range from 10 Neutrals/Ion to greater than 4 x 10^6 Neutrals/Ion [5,22]. The total ESD cross section was measured by monitoring the surface concentration as a function of time, and the relative number of neutrals to ions is not known. For a HOAG to be useful in the study of orbiting spacecraft materials, it must produce almost exclusively neutrals.

In this study, the surface composition of the Ag/0.5% Zr alloy is measured using ISS. In addition, the ESD cross section is determined from AES measurements and the neutral to ion ratio is measured using a mass spectrometer. A preliminary investigation of the effect of primary electron beam angle on the ESD yield is also presented.

Experimental

The alloy used in this study was prepared by vacuum melting a mixture of Ag and 0.5 wt. % Zr in a manner similar to the preparation of the high-purity large-grain silver. The sample was solvent cleaned in an ultrasonic bath with toluene, acetone, trichloroethylene,acetone, and ethanol in that order. The alloy was cleaned in the UHV analysis system by repeated Ar+ sputtering and annealing until no further contaminants

could be detected by AES and ISS. Zirconium is quite reactive to many different compounds such as CO, CO_2, and Cl so care had to be taken to keep the background levels of the reactive contaminants to a minimal level and the sample had to be regularly sputter cleaned.

Oxygen dosing, ESD studies, and surface analysis were all performed in the UHV vacuum system described the appendix. For the ISS analysis, a 100 nA primary beam of 1 keV He^+ was defocussed over a large area to minimize possible sputter damage. A scattering angle of 144° was used and the energy of the scattered ions was analyzed using the PHI model 25-270AR CMA operated in the nonretarding mode. AES data were also taken by using the CMA operated in the nonretarding mode with a primary beam energy of 3 keV. Signal detection was accomplished by applying a 5 kHz oscillation to the outer cylinder and detecting the output of the multiplier with a lock-in amplifier. In this manner, a dN(E)/dE spectrum is obtained. Sample heating for the ISS studies was accomplished by using both radiant heating and electron bombardment from a tungsten filament placed behind the sample. The temperature at which the ISS experiments could be performed was limited to 250°C since the vapor pressure of the silver was so high above this temperature that components in the analysis chamber would be coated with silver and malfunction during the relatively long duration of these heating experiments.

ESD experiments were performed in the ESD vacuum chamber attached to the main vacuum chamber. A schematic of the layout is shown in figure 18. The electron source for both the ion and neutral ESD studies is a PHI grazing incidence angle electron gun whose energy can be varied from 100 eV to 5 keV. All of the ESD for these experiments was performed using a primary beam energy of 1 keV. It was found that the ESD yield increased dramatically in the range from 500 eV to 1 keV. Since the overall objective of these studies is to increase the oxygen atom yield, a 1 keV beam was chosen. Two different analyzers were used for the detection of desorbed particles. For the detection of ions, a specially designed SIMS/ESD analyzer was used. This analyzer consists of a quadrupole mass spectrometer with a retarding-accelerating type energy filter on the front of it. With the combined use of the energy filter and the quadrupole mass analyzer it is possible to determine the individual energy distributions for each mass to charge ratio which is desorbed. The drawback of this analyzer is its inability to detect neutral particles. Since most of the particles desorbed in ESD are neutrals, this results in the loss of much of the signal. In addition, an important parameter in determining the mechanism of the ESD is the ratio of ions to neutrals. For these measurements, an EAI quadrupole mass spectrometer is mounted such that ESD neutral particles can be ionized and detected.

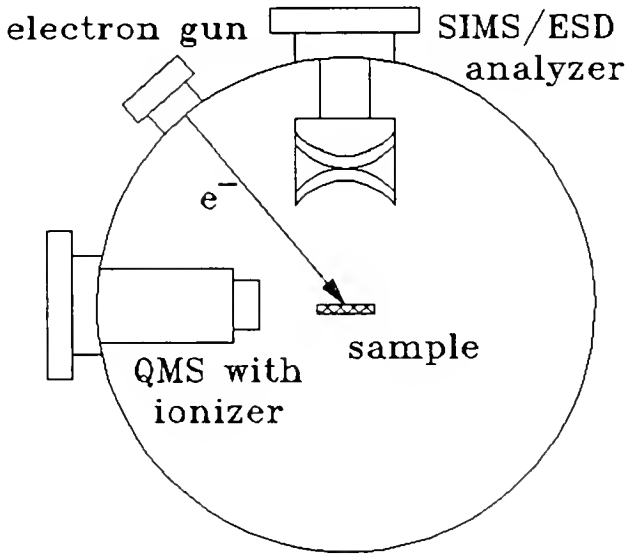

Figure 18. A schematic of the ESD chamber including the QMS and SIMS/ESD analyzer.

One problem with the detection of neutral particles is the large background signal which is present in any vacuum system (fig. 19a). This problem was overcome by utilizing the fact that the desorbing particles have an energy in the 3 to 10 eV range before they enter the ionizer. The ionizer is an electron impact ionizer which operates by passing a beam of 70 eV electrons through an ionization volume which, by electron impact, ionize some fraction of the atoms in the ionization volume. The ions which are formed are then accelerated by a negative potential in the range of 3 to 10 volts. Any ions which have an energy below about 3 eV have a nearly zero probability of getting through the quadrupole. If the ion acceleration potential is reduced to zero, any ions formed from the background gases will not be detected since the background gas molecules have an energy in the thermal range ($\approx$0.03 eV). Particles which are desorbed by ESD however, typically have an energy in the range of 3 to 10 eV and so can be detected (fig. 19b). From figure 19, it can be seen that the relative magnitude of the signals is such that the ESD signal could not be distinguished from the background if the background signal were not removed.

In order to quantify the ion to neutral flux, it is necessary to know the efficiency of the ionizer. This can be calculated from the overall sensitivity of the analyzer to background gases. The sensitivity of the mass spectrometer

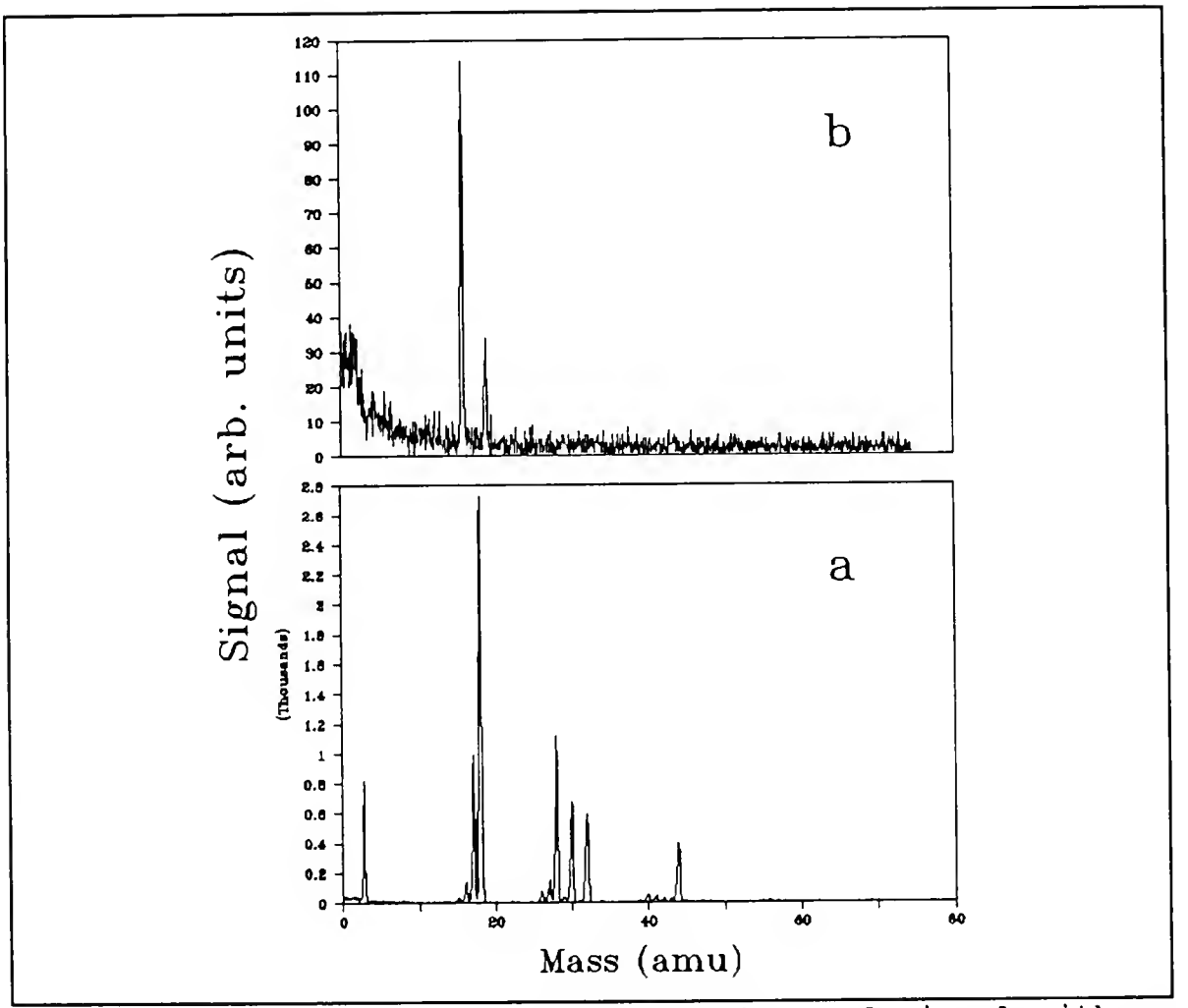

Figure 19. Comparison of: a) the background signal with an ion acceleration potential of 7 V, b) ESD signal with no ion acceleration potential. Note the change in y scale.

to any given gas can be written as [88]

$$S\ (\text{Amps/Torr})\ P\ (\text{Torr}) = I_{out} \qquad (1)$$

where

S is the sensitivity

P is the partial pressure of the gas

I_{out} is the signal detected.

The ideal gas law can be used to convert the pressure to a gas density giving

$$S\ p\ R\ T = I_{out} \qquad (2)$$

where

p is the density

R is the universal gas constant

T is the temperature

For a flux of particles such as the ESD particles the density can be given by

$$p = J_{in} / v_{in} \qquad (3)$$

where

J_{in} is the flux of particles entering the ionizer

v_{in} is the velocity of the particles entering the ionizer

In addition, from the definition of current,

$$I_{out} = J_{out}\ A \qquad (4)$$

where

A is the area of the aperture into the ionizer($0.503 cm^2$)

Substitution of (3) and (4) into (2) gives

$$\frac{J_{out}}{J_{in}} = \frac{S\ R\ T}{v\ A} \qquad (5)$$

Since S is known to be 5 x 10^{-4} Amps/Torr for a 1mA ionizer electron emission of and the energy of the incoming particles are near 5 eV, eqn. (5) can be used to calculate an ionizer efficiency for the desorbing ion flux of 3.2 x 10^{-7} ions/atom. The results presented here were obtained for a 0.2mA ionizer emission so the efficiency for these experiments is 1/5 that for 1mA emission or 6.4 x 10^{-8} ions/ atom.

Preliminary investigation of the dependence of the ESD yield and energy distribution on the electron incidence angle was performed by using the ESD/SIMS head. The angle of the detector with the surface has to be held constant in order to study the dependence of the ESD on the electron incidence angle, since the detected ESD yield is known to be a function of both incidence and detection angle. This was accomplished in the ESD chamber by comparison of ESD ion energy distribution (ESDIED) measurements in which the sample angle was varied 20° to either side of the normal of the analyzer. This is shown in figure 20. In this manner, two spectra were obtained with the same angle to the detector (sample normal 20° from analyzer axis) but with two different electron incidence angles (20° and 60° from the surface normal).

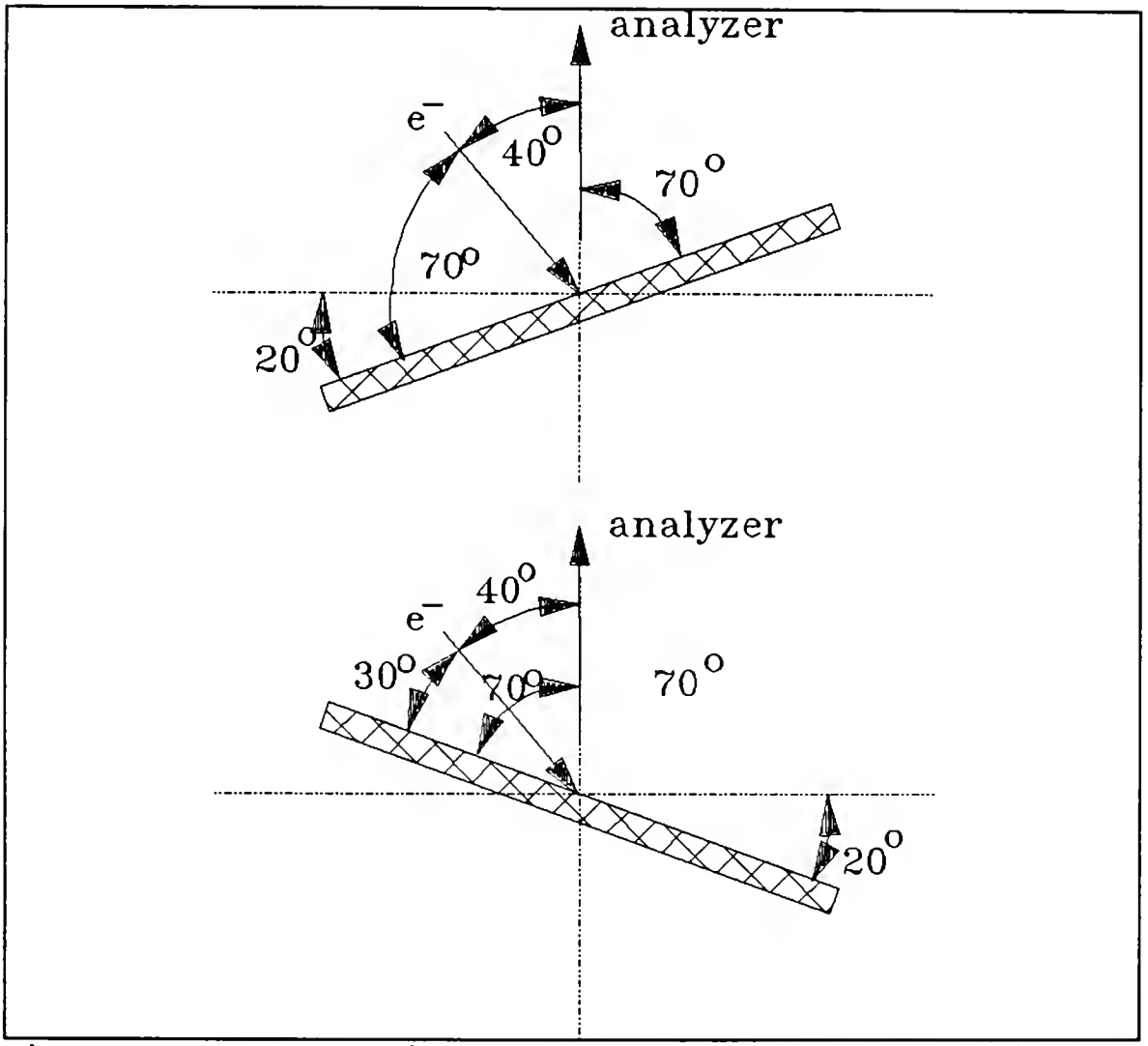

Figure 20. A schematic of the procedure used to examine the dependence of the ESDIED on electron incidence angle while holding the collection angle constant.

Results and Discussion

ISS Data

In order to determine what the composition of the surface might be at the desired operating temperature range of near 500°C, an ISS study was performed in which the sample was sputter cleaned until free from any contaminants and dosed with oxygen at 500°C and 100 Torr for 1 hour. Based on the results for the pure silver, it is believed that this treatment would saturate the sample with oxygen. The sample was then transferred back to the main chamber where it was sputtered until no further changes in the ISS spectrum were noted. This treatment produced a non-equilibrium surface due to the preferential sputtering of the O and to a lesser extent the Zr. The sample was then heated to 250°C and its surface composition was monitored with ISS. As noted previously, the temperature could not be held at 500°C for this experiment due to evaporation of silver. The ISS relative sensitivities could not be calculated for the three component spectra as they could for the O/Ag system because the assumption of constant surface atom density was not valid. In order to quantify the ISS data, the same O/Ag sensitivity of 0.045 as the pure O/Ag case was used. For the relative sensitivity of Zr/Ag the relative sensitivity was calculated using the method of Parilis [86] to be 0.98. Although it was shown that the

O/Ag theoretical relative sensitivity was not accurate, the Zr and Ag are more similar in mass and chemical character so it can be expected that the theoretical relative sensitivity nearly accurate. The surface concentration vs. time for the three components are shown in figure 21. The Zr and O tend to move towards the surface and partially cover the silver. The silver concentration tends to stabilize near 30 at. %. It can be seen from figure 22 that the O to Zr ratio tends toward ZrO_2. The ISS data can be interpreted as either Ag islands on a layer of ZrO_2 or, more likely, a layer of ZrO_2 which does not completely cover the Ag (ie. islands of ZrO_2 on silver).

It is known from the previous studies that the silver saturates with oxygen at about 14%. If islands of ZrO_2 do form over the silver then there would be two separate mechanisms for ESD and, therefore, two peaks in an ESDIED spectrum. ESDIED spectra from oxygen saturated Ag and Ag/0.5% Zr are given in figure 23a and b respectively. Note that the ESDIED from the pure silver shows only one peak at an ion energy of about 5.5 eV but the ESDIED from the alloy shows a peak at about 5 eV and another at about 4 eV. This is confirmation that there are two separate composition regimes, probably ZrO_2 islands on Ag. It should also be noted that the overall yield of O atoms from the Ag/Zr alloy surface is about a factor of 8 larger than that for the pure silver.

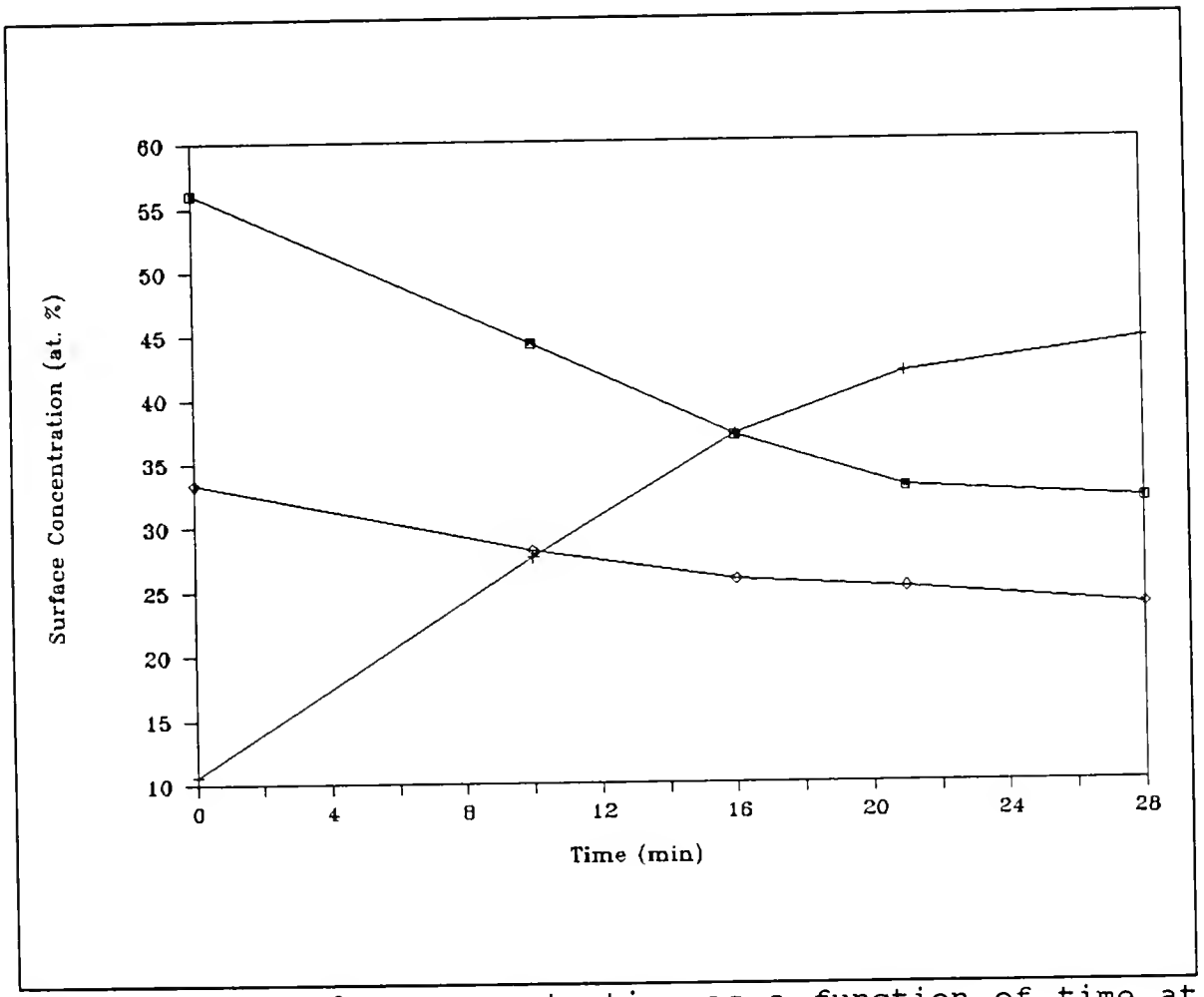

Figure 21. Surface concentration as a function of time at 250°C from ISS.

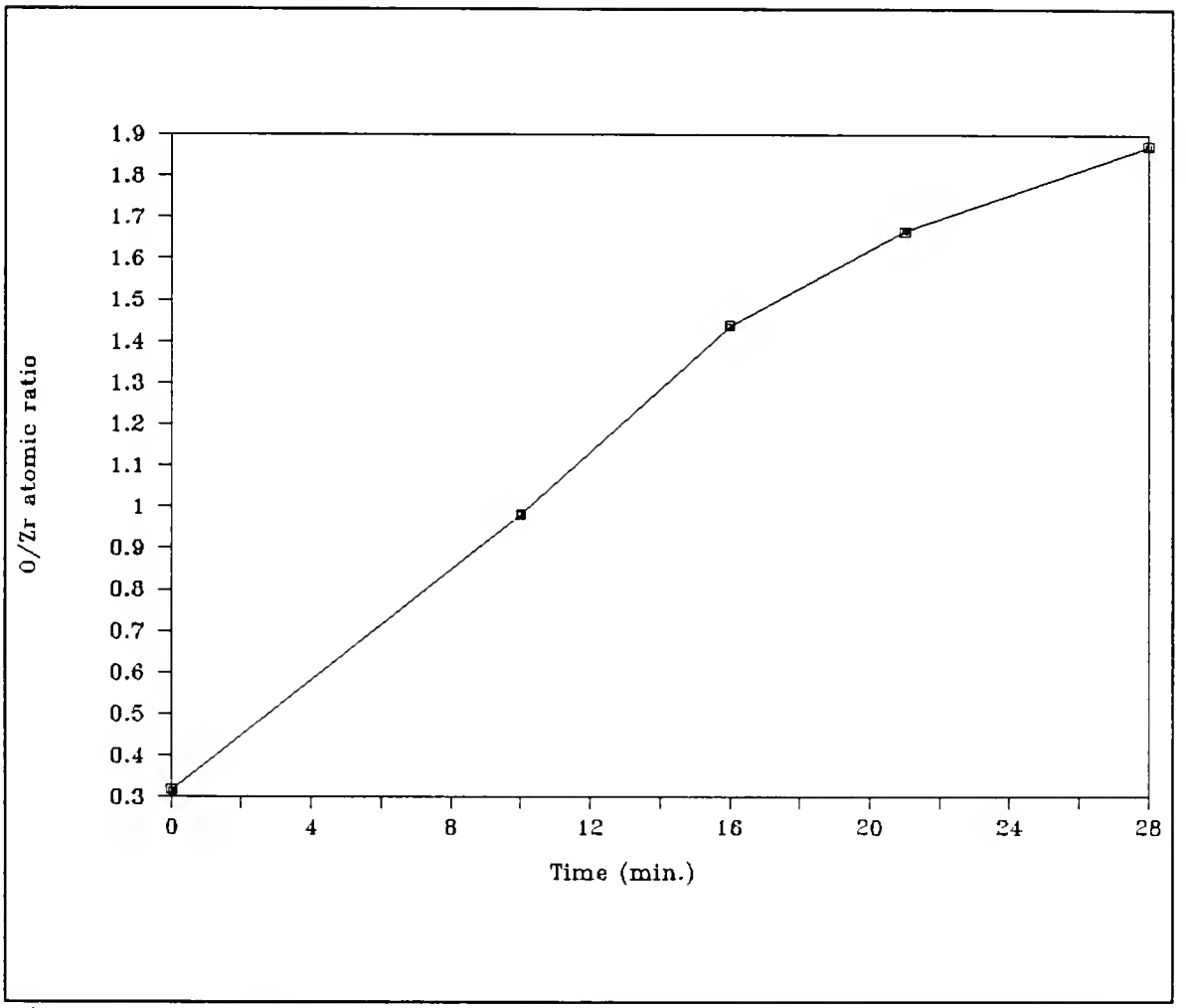

Figure 22. Ratio of O to Zr on the surface as measured by ISS as a function of time at 250°C.

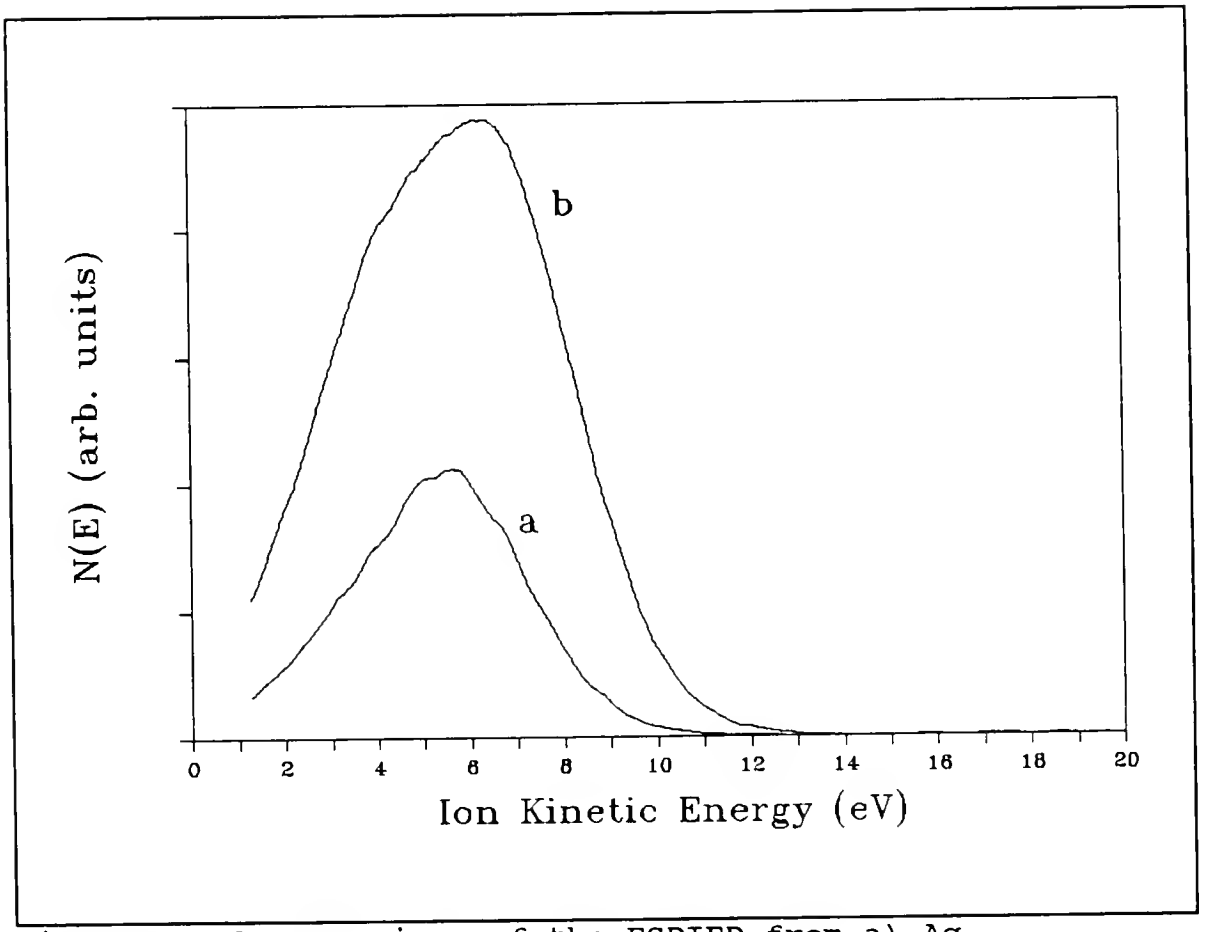

Figure 23. A comparison of the ESDIED from a) Ag, b) Ag/0.5% Zr

Neutral to Ion Ratio Measurement

Some difficulty was encountered in the attempt to measure the neutral to ion cross section. In order to maximize the signal at the QMS the ionizer was placed as close to the sample as possible. Unfortunately, the ionizer was close enough that some of the ionizer electrons struck the sample and produced a background ESD signal which was present whether the main electron beam was on or off. This background signal had to be quantified in order to determine the ratio of neutrals to ions. The background signal was determined by performing several experiments with different combinations of ionizer electrons and primary electrons. The results of these experiments are summarized as follows.

Case #	Primary beam	Ionizer	Mass 16 signal (arb. units)
1	on	off	100
2	on	on	314
3	off	on	143

For case one, the signal detected includes only ions from the primary beam since the ionizer is off. In case 2, the signal detected includes both neutrals and ions from both the primary and background ESD signals. Case three includes only ions and neutrals generated by the background electrons. These relationships can be summarized as follows.

$$I_p = 100 \qquad (6)$$

$$s\ (N_p + N_b) + I_p + I_b = 314 \qquad (7)$$

$$s\ N_b + I_b = 143 \qquad (8)$$

where

I_p is the flux of ions due to the primary beam

N_p is the flux of neutrals due to the primary beam

I_b is the background flux of ions

N_b is the background flux of neutrals

s is the efficiency of the ionizer (6.4×10^{-8})

By solving these equations it can be shown that the neutral to ion ratio is 1.1×10^7 neutrals/ion.

The result that nearly all of the particles desorbed from this surface are neutrals has two major implications. The first is that this surface is quite good for a HOAG with respect to production of neutral oxygen atoms. The second has to do with the mechanism for ESD from this surface. The KF and MGR models generally predict neutral to ion ratios near 1000. The only mechanism proposed in the literature which predicts neutral ratios of greater than 10^7 is the Antoniewicz model which relies on the equilibrium position of the ionized adsorbate state being closer to the surface than the ground state. This mechanism, however, is thought to only occur for adsorbates which are weakly bound to the surface, such as condensed inert gases [21,22]. For the ZrO_2 this is clearly not the case. As was discussed previously, ZrO_2 is a maximal valency oxide, and the KF mechanism is generally favored on

one of the desorption states is due to the ZrO_2. The mechanism for oxygen desorption from the Ag regions is probably the MGR mechanism and, the mechanism for desorption from the ZrO_2 is most likely the KF mechanism.

One possible explanation for the unusually high neutral yield lies in the fact that a 1 keV primary electron beam was used. For a primary beam of electrons of such a high energy, many secondary electrons are produced, which form an electron cloud around the spot where the electron beam strikes the sample. The ions which are desorbed from the surface would have to pass through this electron cloud and would, therefore, have a relatively high probability of being neutralized by electron attachment.

C. Measurement of Total ESD Cross Section

The total cross section for ESD is defined by [5]

$$- d(\theta)/dt = n Q \theta, \qquad (9)$$

where

n is the flux of electrons ($cm^{-2}s^{-1}$)

θ is the surface coverage of the species which is in the binding state affected by ESD. ($atoms/cm^2$)

Q is the total cross section for desorption (cm^2).

This equation may be integrated to give

$$\theta(t)/\theta_o = \exp\{-J\theta t/e\}, \qquad (10)$$

where

J is the electron current density (A/cm^2)

e is the electronic charge (C)

θ_o is the initial coverage.

The overall cross section can be determined from a plot of log $\theta(t)/\theta_o$ vs. time. The surface coverage can be monitored by AES but, a portion of the peak to peak height of the oxygen peak in an Auger spectrum of the oxygen saturated Ag/0.5% Zr alloy is proportional to the surface coverage and part of the signal is due to the oxygen beneath the surface. In order to separate these two signals the sample was kept under the electron beam for several hours until no further change in the oxygen signal was seen. The signal at that point was assumed to be that portion of the AES signal which was due to oxygen beneath the surface and this residual signal was subtracted from the total signal in order to obtain a quantity which was proportional to surface coverage. Substituting the corrected AES signal into eqn. 10 gives

$$\ln\{ (N(t)-N_\infty)/(N_0-N_\infty) \} = -(JQ/e)t \qquad (11)$$

A plot of this quantity vs. time is given in figure 24. From the slope of a linear least squares fit to this data, a total cross section for ESD was found to be 3.9×10^{-19} cm_2.

This cross section is slightly smaller than the O ESD cross section for pure silver which was determined to be 7×10^{-19} cm_2 [1]. This is consistent with the observed total yield for ESD from the alloy which is about 8 times higher than for the pure silver since the oxygen concentration is

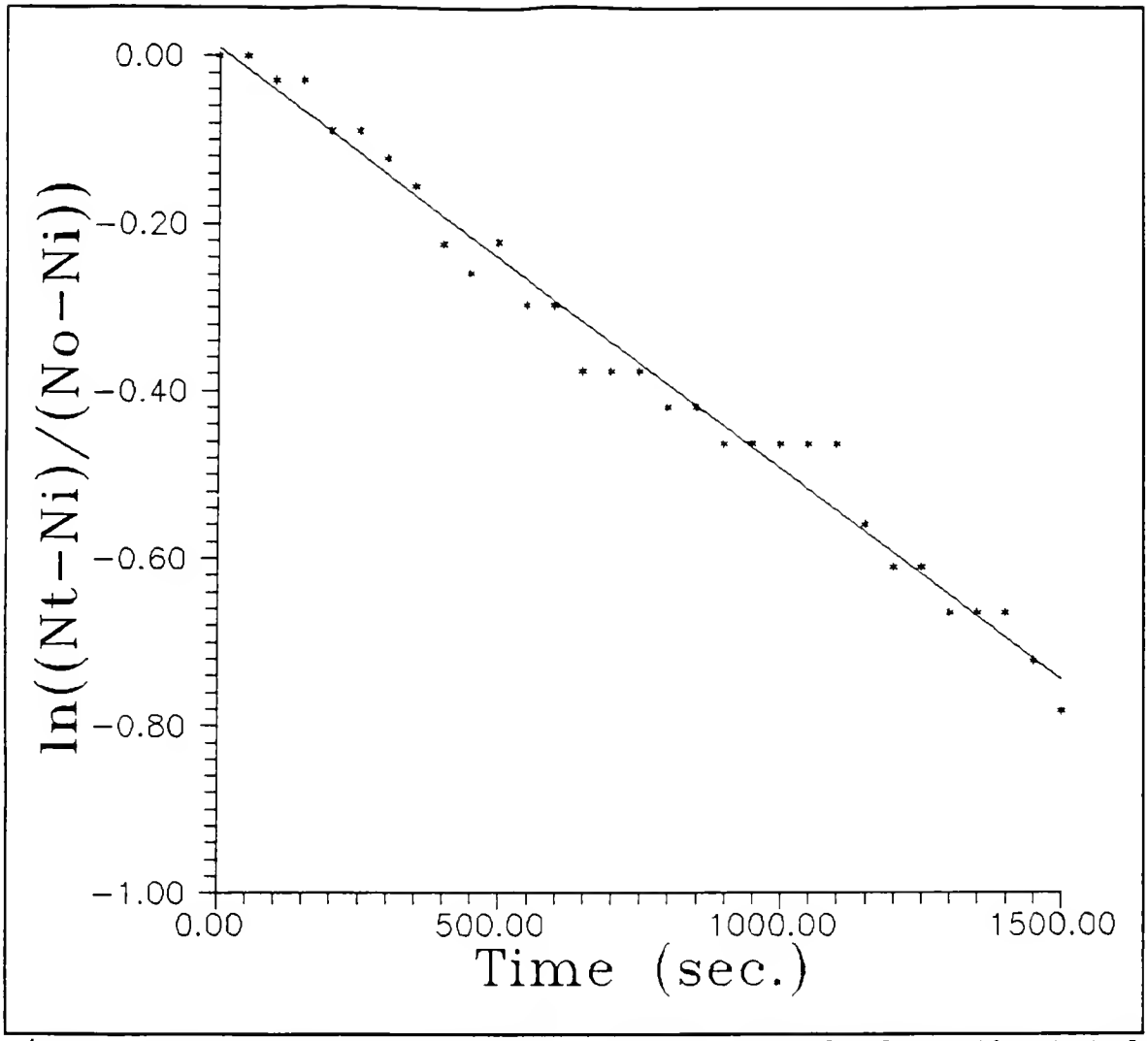

Figure 24. Plot of the AES data used to calculate the total cross section for ESD. Slope of the best fit line is -0.00503.

higher for the fully oxidized alloy surface than that for the pure silver.

Effect of Electron Incidence Angle

The ESDIED for the two electron incidence angles which were obtained for this study are shown in figure 25. Both of the spectra were obtained with the same collection angle but differing incidence angles. The overall ion signal for the more glancing angle of incidence (Fig. 25b) is about three times larger in magnitude than the overall ion yield for the more normal incidence. In addition, the energy maximum of the more glancing incidence spectrum is about 1 eV higher than that for the more normal angle of incidence. The difference in magnitude could be explained by a change in the shape of the electron cloud which would change the neutralization probability, but this would not explain the shift in energy. The differences could be explained by considering the mechanisms for desorption. All of the mechanisms proposed rely on excitation of a bonding orbital by an incoming electron. The bonding orbitals are generally located between the surface atom and the adsorbate. An electron which was approaching the adsorbate bond from above would tend to be partially screened from the bonding orbital by the adsorbate atom while an electron which approaches from a glancing angle would less screened. The glancing electrons would have more access to the bonding orbitals and, perhaps, access to some

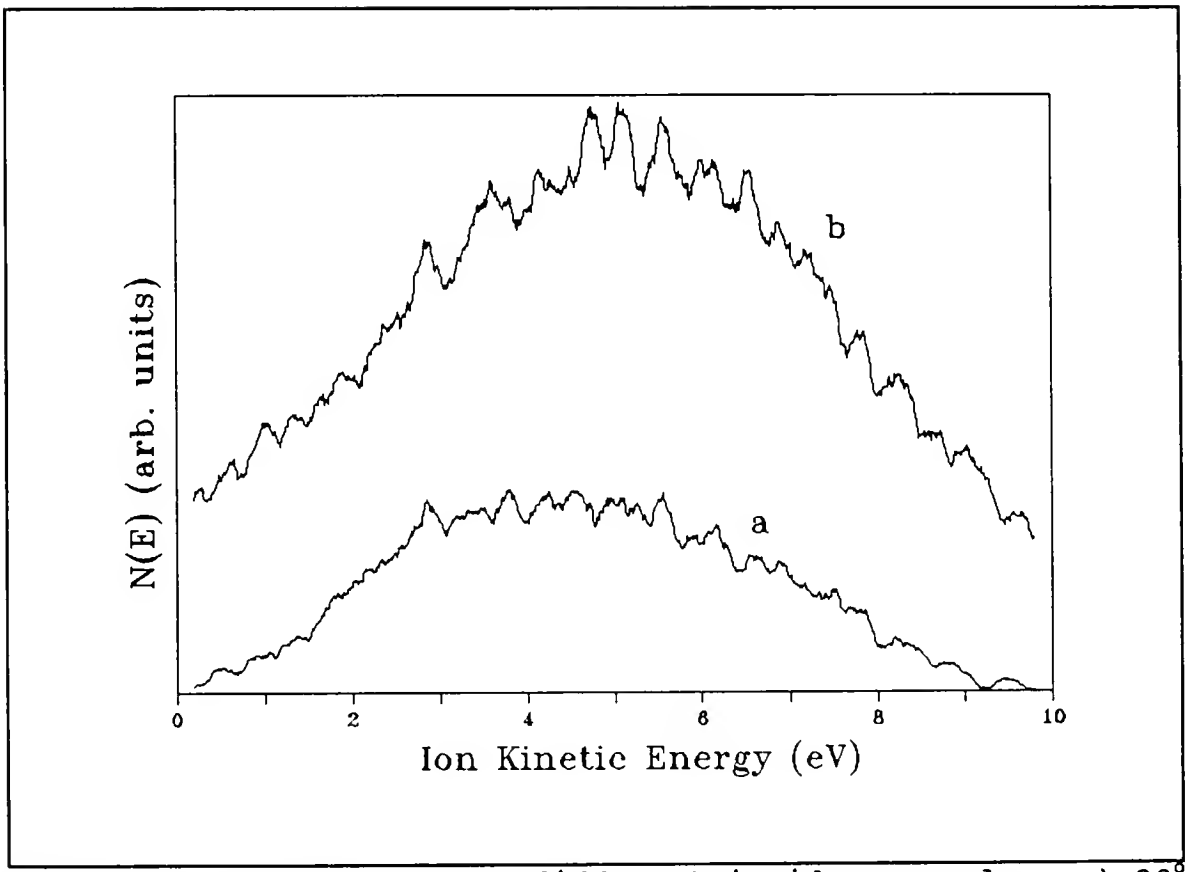

Figure 25. ESDIED for two different incidence angles. a) 20° from surface normal, b) 60° from surface normal.

orbitals which are nearly blocked from the surface normal. The results for this experiment as well as the hypothesis to explain them are preliminary and further investigation into this phenomenon is being planned.

Summary and Conclusions

All of the studies presented in this chapter indicate that the Ag/0.5% Zr alloy will make a surface which is superior to pure Ag with regard to generation of a hyperthermal neutral oxygen atom beam by ESD. The ratio of neutrals to ions for ESD of oxygen by 1 keV electrons from this surface is more than 1×10^7. The energy distribution of desorbing oxygen from the alloy is broader than that for the pure silver but it is still centered near 5 eV and shows a total ESD oxygen yield about 8 times higher than pure silver. The cross section which was measured for the alloy is about half that measured of O ESD from silver but the higher concentrations of oxygen in the alloy cause the oxygen ESD yield to be higher. A more grazing electron incidence angle was shown to give an increased oxygen ion yield and slightly higher energy maximum but the reasons for this are not yet well understood.

APPENDIX

DESCRIPTION OF THE ULTRAHIGH VACUUM SURFACE FACILITY

A top view of the system is shown in Figure 26. This system has many unique capabilities for the study of surfaces. A system has been developed which consists of a sample preparation chamber, a pretreatment chamber, and the UHV analysis chamber. A sample manipulator system has been developed which makes it possible to move the sample between the various chambers and heat the sample in the preparation or analysis chamber. It is also possible to prepare model catalysts in a highly controlled atmosphere with intermediate surface characterizations. Then, the sample can be moved from the vacuum system and inserted into a high pressure reactor and back into the UHV system for analysis without exposure to air.

It is possible to prepare numerous types of catalytic surfaces in this type of system. Many of our studies have involved electrochemically prepared catalysts such as tin oxide- or titania- supported platinum. With this system oxide surfaces can be prepared and characterized in the UHV system. Facilities for metallization are also contained in the

preparation chamber so that mixed oxide catalysts and supported metal catalysts can be prepared totally within the system. Furthermore, the same facilities which are used for catalyst preparation can be used for treatment of materials with high pressures of gases at temperatures up to ≈800 C.

The system utilizes ion pumping and Ti sublimation pumping to reach a base pressure in the 10^{-11} Torr range. A turbomolecular pump is used to rough the system, pump inert gas away after sputtering or performing ion scattering spectroscopy (ISS), and differentially pump other portion of the system. A PHI Model 25-270AR double-pass CMA charged-particle energy analyzer is suspended vertically from port 6. Port 5 contains a manipulator with capabilities for moving, heating, and cooling the sample. The sample is placed on this manipulator by a long stroke manipulator after sample preparation and pretreatment.

Many surface techniques are included in this UHV system (see Table I). The CMA is used both as a charged particle energy analyzer and as a time-of-flight mass spectrometer. Numerous sources are mounted in the ports focusing at the CMA focal point including an ion gun, an ultraviolet photon generator, an X-ray source, electron guns and a molecular beam doser. This allows us to perform many techniques using the CMA including X-ray photoelectron spectroscopy (XPS), Auger electron spectroscopy (AES) and scanning Auger microscopy

(SAM), electron energy loss spectroscopy (ELS), Auger electron appearance potential spectroscopy (AEAPS), electron stimulated desorption with angular resolution and energy analysis (ESD, ESDIAD, ESDIED), ultraviolet photoemission spectroscopy (UPS), ion scattering spectroscopy (ISS), and secondary ion mass spectrometry (SIMS). This chamber also contains a mass spectrometer and a secondary electron detector so that we can perform temperature programmed desorption (TPD), isotope exchange experiments, and work function measurements. It is possible to perform many of these techniques in an angularly resolved manner over a very broad temperature range from that of liquid nitrogen to above 1200 C.

Table I

Available Techniques

I. Cylindrical Mirror Analyzer

- *A. X-ray Photoelectron Spectroscopy
- *B. Ultraviolet Photoemission Spectroscopy (UPS)
- *C. Auger Electron Spectroscopy (AES)
- D. Scanning Auger Microscopy (SAM)
- *E. Electron Energy Loss Spectroscopy (ELS)
- F. Auger Electron Appearance Potential Spectroscopy (AEAPS)
- *G. Electron Stimulated Desorption (ESD, ESDIED, ESDIAD)
- H. Ion Scattering Spectroscopy (ISS)
- I. Depth Profiling

II. Others

- A. Work Function Measurements
- B. Temperature programmed Desorption
- C. Isotope Exchange Experiments
- D. Secondary Ion Mass Spectrometry (SIMS and Tandem SIMS)
- E. Gas Dosing
- F. Heating > 1500 C
- G. Cooling to 10 K
- H. Inverse Photoelectron Spectroscopy
- I. Metal Deposition
- J. High Pressure Pretreatment

*Can be performed in the angle-resolved mode

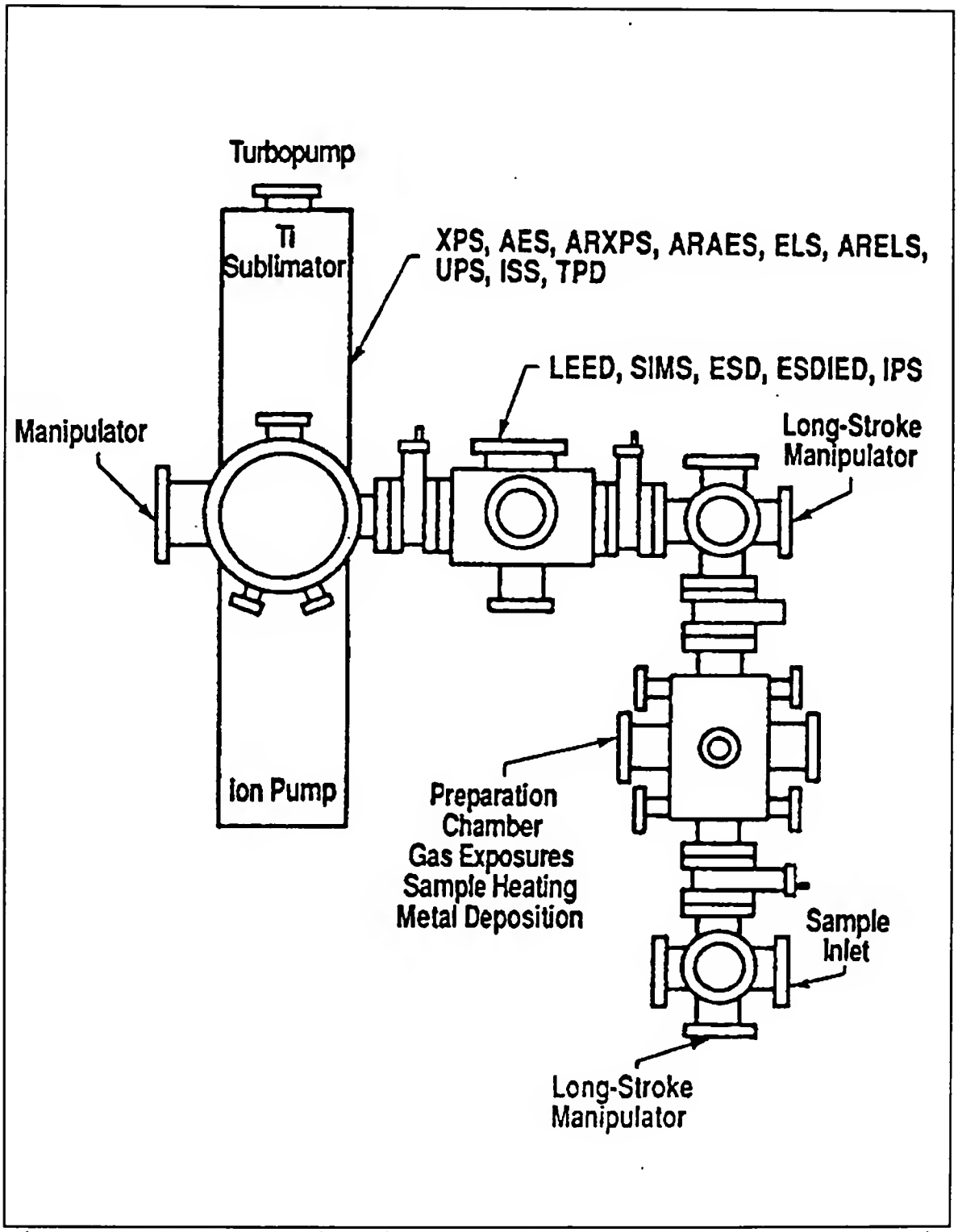

Figure 26. Schematic diagram of the vacuum system used in these studies.

REFERENCES

1. R.A. Outlaw, W.K. Peregoy, G.B. Hoflund, and G.R. Corallo, NASA technical paper 2668, April 1987

2. R.A. Outlaw and F.J. Brock, J. Vac. Sci. Tech 14(1977)1269

3. W. Eichenauer and G. Muller, Z. Met. Kd., 53(1962)321

4. T.A. Ramanarayanan and R.A. Rapp, Metall. Trans. 3(1972)3239

5. T.E. Madey and J.T. Yates, Jr., J. Vac. Sci. Technol., 8(1971)525

6. G.B. Hoflund, Scanning Elect. Microsc., (1985)1391

7. R. Gomer in Desorption Induced by Electronic Transitions DIET I, p. 80, Eds. N.H. Tolk, M.M. Traum, J.C. Tully, and T.E. Madey, Springer-Verlag, New York, NY, 1983

8. P. Feulner, S. Auer, T. Muller, A. Puschmann, and D. Menzel in Desorption Induced by Electronic Transitions DIET III, p. 58, Eds. R.H. Stulen and M.L. Knotek, Springer-Verlag, New York, NY, 1988

9. G.E. Moore, J. Appl. Phys. 32(1961)1241

10. D.R. Sandstrom, J.H. Leck, and E.E. Donaldson, J. Appl. Phys. 38(1967)2851

11. T.E. Madey and J.T. Yates, Jr., Surface Sci., 11(1968)327

12. D.A. Degras and J. Lecante, Nuovo Cimento Suppl. 5(1967)598

13. P.A. Redhead, Nuovo Cimento Suppl., 5(1967)586

14. W. Ermrich, Nuovo Cimento Suppl., 5(1967)580

15. J.T. Yates Jr., T.E. Madey, and J.K.Payn, Nuovo Cimento Suppl., 5(1967)558

16. P.A. Redhead, Can. J. Phys., 42(1964)386

17. J.W. Coburn, Surface Sci., 11(1968)61

18. S. Auer, P. Feulner, and D. Menzel, Phys. Rev. B, 35(1987)7752

19. P. Feulner and D. Menzel, Phys. Rev. Lett., 53(1984)671

20. E.R. Moog, J. Ungris, and M.B. Webb, Surface Sci., 134(1983)849

21. Q.J. Zhang and R. Gomer, Surface Sci. 109(1981)567

22. Q.J. Zhang, R. Gomer, and D.R. Bowman, Surface Sci. 129(1983)535

23. R.A. Outlaw, G.B. Hoflund, and G.R. Corallo, App. Surface Sci. 28(1987)235

24. D. Menzel in Desorption Induced by Electronic Transitions DIET I, Eds. N.H. Tolk, M.M. Traum, J.C. Tully, and T.E. Madey, Springer-Verlag, New York, NY, 1983

25. P. Feulner, S. Auer, T. Muller, A Puschmann, and D. Menzel in Desorption Induced by Electronic Transitions DIET III, p. 61, Eds. R.H. Stulen, and M.L. Knotek, Springer-Verlag, New York, NY 1988

26. P.R. Antoniewicz, Phys Rev. B 21(1980)3811

27. J.S. Hammond, S.W. Gaarenstroom, and N. Winograd, Anal. Chem., 47(1975)2193

28. G. Schon, Acta Chemica Scandinavica, 27(1973)2623

29. R.E. Kenson and M. Lapkin, J. Phys. Chem.,74(1970)1493

30. P. Harriott, J. Catalysis, 21(1971)56

31. N.W. Cant and W.K. Hall, J. Catalysis, 52(1978)81

32. A.L. Larrabee and R.L. Kuczkowski, J. Catalysis., 52(1978)72

33. T. Inui and Y. Tanabe, J. Catalysis, 52(1978)375

34. H. Kanoh, T. Nishimura, and A. Ayame, J. Catalysis, 57(1979)372

35. H.R. Dettweiler, A. Baiker, and W. Richarz, Helvetica Chimica Acta, 62(1979)1689

36. S. Kagawa, M. Iwamoto, H. Mori, and Tetsuro Selyama, J. Pys. Chem. 85(1981)434

37. P. Vishnu Kamath, K. Prabhakaran, and C.N.R. Rao, Surface Sci. 146(1984)L551

38. P.J. Goddard and R.M. Lambert, Surface Sci., 107(1981)519

39. R.B. Grant and R.M. Lambert, Surface Sci. 146(1984)256

40. T.E. Felter, W.H. Weinberg, P.A. Zhdan, and G.K. Boreskov, Surface Sci. 97(1980)L313

41. R.B. Grant and R.M. Lambert, Surface Sci., 146(1984)256

42. H.A. Engelhardt and D. Menzel, Surface Sci.,57(1976)591

43. J. Eickmans and A. Otto, Surface Sci., 149(1985)293

44. C.T. Campbell, Surface Sci., 157(1985)43

45. C.T. Campbell and M.T. Paffett, Surface Sci. 143(1984)517

46. K. Bange, T.E. Madey, and J.K. Sass, Surface Sci., 152/153(1985)

47. M. Bowker, M.A. Barteau, and R.J. Madix, Surface Sci., 92(1980)528

48. C. Benndorf, M. Franck, and F. Thieme, Surface Sci., 128(1983)417

49. C. Backx, C.P.M. DeGroot, P. Biloen, and W.M.H. Sachtler, Surface Sci. 128(1983)81

50. C. Backx, C.P.M. DeGroot, and P. Biloen, Surface Sci., 104(1981)300

51. C.T. Au, S. Singh-Boparai, M.W. Roberts, and R.W. Joyner, J. Chem. Soc., Faraday Trans. 1, 79(1983)1779

52. I.E. Wachs and S.R. Kelemen, J. Catalysis, 68(1981)213

53. R. Sporken, P.A. Thiry, J.J. Pireaux, R. Caudano, and A. Adnot, Surface Sci. 160(1985)443

54. C.T. Campbell and M.T. Paffett, Surface Sci. 139(1984)396

55. G. Rovida, F. Pratesi, M. Maglietta, and E. Ferroni, J. Vac. Sci. Tech, 9(1971)796

56. S. Kagawa, M. Iwamoto, and S. Morita, 78(1982)143

57. G. Rovida, F. Pratesi, M. Maglietta and E. Ferroni, Surface Sci., 43(1974)230

58. G. Rovida amd F. Pratesi, Surface Sci. 52(1975)542

59. W. Heiland, F. Iberl, E. Taglauer, and D. Menzel, Surface Sci. 53(1975)383

60. M. Kitson and R.M. Lambert, Surface Sci., 109(1981)60

61. A. Puschmann and J. Haase, Surface Sci., 144(1984)559

62. K.C. Prince and A.M. Bradshaw, Surface Sci., 126(1983)49

63. W. Krakow, Surface Sci., 140(1984)137

64. L. Lefferts, J.G. van Ommen, and J.R.H. Ross, App. Catalysis, 31(1987)291

65. M. Stoukides and C.G. Vayenas, J. Catalysis, 64(1980)18

66. M. Peukert, Surface Sci., 146(1984)329

67. B. Reihl, R.R. Schlittler, and H. Neff, Surface Sci., 152/153(1985)231

68. S. Kagawa, M. Iwamoto, and S. Morita, J. Chem. Soc., Faraday Trans. 1, 78(1982)143

69. F.K. Moghadam and D.A. Stevenson, J. Electrochem. Soc., 133(1986)1329

70. N. Ting, Y. Qingliang, and Y. Yiying, Surface Sci., 206(1988)L857

71. Y. Kuk and L.C. Feldman, Phys. Rev. B, 30(1984)5811

72. H. Rickert and R. Steiner, Z. Phys. Chem. 49(1966)127

73. E.H. Kolosov, H. Starkovscii, and B.M. Gryanznow, Zh. Fiz. Khim., 48(1974)1861

74. B.M. Gryaznov, C.G. Gul'yanova, and C. Kanizius, Russ. J. Phys. Chem. 47(1973)1517

75. R.E. Coles, Br. J. Appl. Phys., 14(1963)342

76. J. Crank, Mathematics of Diffusion, 2nd ed., p. 42 Oxford University Press, Oxford, 1967

77. R.A. Outlaw, W.K. Peregoy, and G.B. Hoflund, NASA Tech. Pub. 2755(1987)

78. L.C. Beavis, Rev. Sci. Instrum., 43(1972)122

79. D.J. Mitchell, J.M. Harris, R.C. Patrick, E.P. Boespflug, and L.C. Beavis, J. Appl. Phys., 53(1982)970

80. H.H. Johnson and R.W. Lin, in Proceedings of the 3rd International Conference on Effect of Hydrogen on the Behavior of Material, Eds. I.M. Bernstein and A.W. Thompson, AIME, New York, NY, 1981

81. R.E. Hoffman and D.J. Turnbull, J. Appl. Phys. 22(1951)634

82. W. Segeth, J.H. Wijngaard, and G.A. Savatzky, Surface Sci., 194(1988)615

83. Y. Kuk and L.C. Feldman, Phys. Rev. B. 30(1984)5811

84. G.B. Hoflund, D.A. Asbury, C.F. Corallo, and G.R. Corallo, J. Vac. Sci. Technol. A 6(1988)70

85. G.B. Hoflund and V. Young, Submitted to Surface Sci.,1990

86. E.S. Parilis in Proceedings of the 7th International Conference on Phenomena in Ionized Gases Vol. 1, Belgrade, 1965, p. 129, Eds. B. Perovic and D. Tosic, Gradevinska Knjiga Publishing House, Belgrade, 1966

87. A. Zangwill, Physics at Surfaces, Cambridge University Press, New York, NY, 1988

88. QUAD 250 Residual Gas Analyzer Instruction Manual, Electronics Associates, Inc., Palo Alto, California, 1965

BIOGRAPHICAL SKETCH

The author was born on July 10, 1962, in Chattanooga, Tennessee, to A. Rogers and Mary C. Davidson. Soon after his birth, his parents moved back to their native Florida. The author was raised in Seminole, Florida, where he attended Seminole High School and graduated in May, 1980. He received a national merit scholarship to attend the University of Florida in Gainesville. During his undergraduate education, he worked as a lab assistant for Professor Herbert A. Laitinen in the Department of Chemistry. While working for Professor Laitinen, the author had some exposure to the work of Professor Gar B. Hoflund with the Chemical Engineering Department in the field of surface analysis. After graduating with a B.S. in chemistry, the author chose to attend graduate school in the Department of Chemical Engineering, in order to learn the science of probing the outermost layers of solid materials. In May 1986, the author was awarded a Master of Engineering in chemical engineering. The author plans to receive his Ph.D. in May, 1990.

I certify that I have read this study and that in my opinion it conforms to acceptable standard of scholarly presentation and is fully adequate, in scope and quality, as a dissertation for the degree of Doctor of Philosophy.

Gar B. Hoflund

Gar B. Hoflund, Chairman
Professor of Chemical
Engineering

I certify that I have read this study and that in my opinion it conforms to acceptable standard of scholarly presentation and is fully adequate, in scope and quality, as a dissertation for the degree of Doctor of Philosophy.

Herbert A. Laitinen
Graduate Research
Professor of Chemistry

I certify that I have read this study and that in my opinion it conforms to acceptable standard of scholarly presentation and is fully adequate, in scope and quality, as a dissertation for the degree of Doctor of Philosophy.

Timothy J. Anderson

Timothy J. Anderson
Professor of Chemical
Engineering

I certify that I have read this study and that in my opinion it conforms to acceptable standard of scholarly presentation and is fully adequate, in scope and quality, as a dissertation for the degree of Doctor of Philosophy.

Gerasimos K. Lyberatos
Associate Professor of
Chemical Engineering

I certify that I have read this study and that in my opinion it conforms to acceptable standard of scholarly presentation and is fully adequate, in scope and quality, as a dissertation for the degree of Doctor of Philosophy.

Vaneica Y. Young
Associate Professor of Chemistry

This dissertation was submitted to the Graduate Faculty of the College of Engineering and to the Graduate School and was accepted as partial fulfillment of the requirements for the degree of Doctor of Philosophy.

May, 1990

for Herbert A. Bern
Winfred M. Phillips
Dean, College of Engineering

Madelyn M. Lockhart
Dean, Graduate School